Fish and Shellfish Immunology 177 (2026) 111584

Contents lists available at ScienceDirect

Fish and Shellfish Immunology

journal homepage: www.elsevier.com/locate/fsi

Full length article

Identification of two MAPK transcripts in the colonial ascidian *Botryllus schlosseri*: involvement in immune and stress responses and potential roles in colony growth

Laura Drago [a], Francesca Frisoni [b], Gianfranco Santovito [a], Loriano Ballarin [a,*]

[a] Department of Biology, University of Padova, Via Ugo Bassi 58/B, Padova, 35131, Italy
[b] Department of Biology, University of Konstanz, Universitätsstraße 10, Konstanz, 78464, Germany

ARTICLE INFO

Keywords:
MAPK pathways
Blastogenetic cycle
Botryllus schlosseri
Oxidative stress
Stress granules
Post-transcriptional regulation

ABSTRACT

Mitogen-activated protein kinase (MAPK) pathways are evolutionarily conserved signalling cascades that regulate fundamental cellular processes such as proliferation, differentiation, and stress responses. In the colonial ascidian *Botryllus schlosseri*, MAPK activity is required for efficient phagocytosis of non-self cells or particles. In the present study, we identified two novel MAPK transcripts in *B. schlosseri* and analysed their modulation during the colonial blastogenetic cycle under various experimental conditions. Since phagocytic activity is essential for the cyclical renewal of the colony throughout the blastogenetic cycle, we also investigated the effects of colony exposure to MAPK inhibitors, PD98059 and SP600125, targeting the ERK and JNK signalling pathways, respectively. Colonies were microinjected with the inhibitors, and changes in morphology and transcriptional profiles were analysed. The inhibition of MAPK activity altered colony development and modulated the expression of genes associated with oxidative stress protection (*sod*, *gpx-5*) and stress granule dynamics (*tiar*, *ttp*), processes involved in post-transcriptional regulation. These findings suggest that MAPK signalling is indispensable for the proper progression of the blastogenetic cycle in *B. schlosseri*, integrating oxidative stress defence and post-transcriptional control to maintain colony homeostasis.

1. Introduction

Mitogen-activated protein kinases (MAPKs) are a family of enzymes that covalently and reversibly attach phosphate groups onto serine and threonine residues of specific target proteins within the cell. Through the phosphorylation of other protein kinases, phospholipases, cytoskeletal proteins and transcription factors, MAPKs can modulate enzymatic activities, protein-protein or protein-molecule interactions, as well as their susceptibility to proteolytic degradation. In this way, they control important cellular processes such as metabolism, movement, meiosis and mitosis, apoptosis and gene expression [1,2]. Signal transduction usually begins with the activation of Ras/Rho small GTPases, which leads to the sequential phosphorylation of MAP kinase kinases (MAPKKKs), MAP kinase kinases (MAPKKs) and, finally, MAPKs [3,4]. Activated MAPKs can phosphorylate various substrates in the cytosol and nucleus leading to changes in protein function and gene expression [5].

From yeast to humans, three main conserved subfamilies of MAPKs have been identified: extracellular signal-regulated kinases (ERKs), c-Jun NH2-terminal kinases (JNKs) and p38s. Two groups of ERK family members have been described: the classic ERKs (ERK-1 and ERK-2, alias MAPK-3 and MAPK-1, respectively) and the larger ERKs (e.g., ERK-5, alias MAPK-7) that contain an extended C-terminal sequence in addition to their kinase domain [6]. ERK-1 and ERK-2 respond primarily to growth factors and mitogens to induce cell growth and differentiation [7,8]. The JNK family includes JNK-1, JNK-2, and JNK-3 (also known as MAPK-8, MAPK-9 and MAPK-10, respectively) [9]. They are activated by environmental stress, inflammatory cytokines, and growth factors and play important roles in apoptosis, inflammation, cytokine production, and metabolism [10,11]. p38α, p38β, p38γ, and p38δ (also known as MAPK-14, MAPK-11, MAPK-12 and MAPK-13, respectively), are members of the p38 family activated by environmental stress and inflammatory cytokines [12]. The activation of p38s is associated with inflammation, apoptosis, cell differentiation, and cell cycle regulation [13,14]. The three main MAPK subfamilies have been extensively

* Corresponding author.
E-mail addresses: laura.drago@unipd.it (L. Drago), ffrisoni@ab.mpg.de (F. Frisoni), gianfranco.santovito@unipd.it (G. Santovito), loriano.ballarin@unipd.it (L. Ballarin).

https://doi.org/10.1016/j.fsi.2026.111584
Received 16 March 2026; Received in revised form 19 June 2026; Accepted 6 July 2026
Available online 9 July 2026

Abbreviations used in the text

A	adenine
ANOVA	one-way analysis of variance
BIC	Bayesian information criterion
cAIC	Akaike information criterion
CDS	coding DNA sequence
CTAB	cetyltrimethylammonium bromide
DAB	3,3′-diaminobenzidine
EC	early-cycle
ef	elongation factor
ERK	extracellular signal-regulated kinase
FSW	0.45 μm-filtered seawater
GPX-5	glutathione peroxidase 5
HRP	horseradish peroxidase
JNK	c-Jun NH2-terminal kinase
LC	late-cycle
LPS	lipopolysaccharide from Gram-negative bacteria
MAPK	mitogen-activated protein kinase
MAPKK	MAP kinase
MAPKKK	MAP kinase kinase
MC	mid-cycle
MCMC	Markov chain Monte Carlo
MEGA	molecular evolutionary genetics analysis
MK2	MAPK-activated protein kinase 2
MUSCLE	multiple sequence comparison by log-expectation
P-bodies	processing bodies
PBS	phosphate-buffered saline
qRT-PCR	quantitative real-time PCR
RBP	RNA-binding protein
ROS	reactive oxygen species
SG	stress granule
SOD	superoxide dismutase
TIAR	TIA-1 related nucleolysin
Tm	melting temperature
TNF	tumor necrosis factor
TO	take-over
TTP	tristetraprolin
U	uridine
UTR	untranslated region

studied in mammals.

As regards their roles in immunity, ERK is required for immunocyte proliferation, whereas JNK and p38 are the major players in stress responses and innate immunity [15–18]. Invertebrates rely only on innate immunity for their defence and the recruitment of MAPKs in innate immune responses has been described in both spiralians and ecdysozoans. In spiralians, the involvement of p38 in immune responses has been described in bivalve and gastropod species [19,20], whereas ERK, together with p38, is activated by non-self recognition in the gastropod *Littorina littorea* [20]. ERK and JNK are involved in immune responses of the scallop *Patinopecten yessoensis* [21]. ERK is also required for proper phagocytosis in the gastropod *Limnaea stagnalis* [22]. As far as ecdysozoans are concerned, p38 and JNK signalling pathways exert a pivotal role in defence towards bacterial infections in nematodes [23–26]. In addition, p38 and JNK are important for the modulation of immune responses towards bacteria, fungi and viruses in insects [26–29]. Among deuterostomes, the transcription of MAPK genes is upregulated in the sea cucumber *Apostichopus japonicus*, upon exposure of whole animals or isolated coelomocytes to *Vibrio splendidus* [30].

Tunicates are invertebrate chordates representing the sister group to vertebrates [31]. They include sessile ascidians and pelagic thaliaceans and larvaceans [32,33]. Except for a few papers on immunocytes and immune responses in thaliaceans [34,35], most of the data of immune responses in tunicates come from studies on ascidians. Here, the main effectors of immune responses are the circulating immunocytes, represented by phagocytes and cytotoxic granular cells [36]. Ascidians respond to the recognition of non-self (either microbes or foreign/self altered cells) with inflammation, phagocytosis or encapsulation. Cytotoxic cells represent the most abundant circulating haemocyte type and store the enzyme phenoloxidase within their granules [37]. Upon recognition of non-self, phenoloxidase is released and triggers the inflammatory reaction observed *in vitro* in solitary ascidians [38–40] and *in vivo* in colonial species, along the contacting borders of genetically incompatible colonies during the allorejection reaction of botryllid ascidians [41–45].

Botryllus schlosseri is a colonial ascidian widely used as a model organism for the study of innate immune responses [46]. In a previous study, we demonstrated that *in vitro* phagocytosis of target yeast cells in the colonial ascidian *Botryllus schlosseri* requires MAPK signalling pathways [47]. In addition, in this species, sustained oxidative stress leads to the impairment of phagocytosis and death of phagocytes [48,49].

In this study, we mined the available *Botryllus* databases looking for MAPK genes. We identified and characterised two MAPK genes that exhibit similarity to the chordate ERK-2 and JNK-1 genes and are expressed by *Botryllus* phagocytes. We then evaluated their involvement in phagocytosis by inhibiting ERK and JNK activity with PD98059 and SP600125, respectively. In agreement with previous studies, we observed a reduction in phagocytic activity associated with the inhibition of the ERK and JNK pathways. To confirm the effectiveness of the inhibitors in modulating the target proteins, we carried out immunoblot analyses and measured changes in the percentage of immunopositive haemocytes stained with anti-pERK and anti-pJNK antibodies after incubation with yeast, used as an immune challenge, in the presence of the respective inhibitors. Since MAPK pathways can be activated by reactive oxygen species, we also studied the modulation of the transcriptional activity of the two identified MAPK genes by cadmium, zinc and copper (a non-essential metal and two essential metals, respectively), known inducers of oxidative stress in ascidians [50–52], and LPS, a bacterial molecule known to act as an inflammatory inducer in ascidians [53,54]. Moreover, as MAPKs can influence the activity of stress-related genes, we studied the effects of the above-reported inhibitors on the transcription of four previously identified *Botryllus* genes involved in both the response to oxidative stress (*bssod* and *bsgpx-5*) [51] and stress granule (SG) formation (*bstiar* and *bsttp*) [55,56]. In addition, since phagocytic activity is required for the progression of the colonial blastogenetic cycle [57], we evaluated the effects of the two MAPK inhibitors on the blastogenetic cycle. Our findings suggest that the two MAPK genes play important roles in the progression of the blastogenetic cycle and in the modulation of oxidative stress and SG dynamics.

2. Materials and methods

2.1. Animals

Colonies of *B. schlosseri* were collected in Chioggia, in the southern part of the Venice Lagoon, detached from solid substrates with a razor blade and transferred onto glass slides. They were kept in aerated aquaria filled with 0.45 μm-filtered seawater (FSW), in thermostatic rooms at 19 °C under a 12 h light/12 h dark cycle, and fed every other day with *Tetraselmis chuii* and *Dunaliella* sp.

In a colony, adult zooids are grouped in star-shaped systems with a common cloacal siphon in the centre of each system. All the zooids share the tunic and the colonial circulatory system. Colonies undergo periodic

(weekly at 19 °C) generation changes, known as take-overs (TOs), during which adult zooids are progressively resorbed and replaced by their buds (second generation of the colony), which bear budlets (third generation of the colony). The interval between two consecutive TOs is defined as the blastogenetic cycle. During the TO, lasting 24-36 h, diffuse cell death by apoptosis occurs in cells of adult zooids [58,59]. Circulating phagocytes infiltrate adult zooid tissues to remove senescent cells, a process essential for the proper progression of the blastogenetic cycle [57]. A blastogenetic cycle includes various colonial developmental phases [60]. The phases that follow or precede the TO by more than one day are collectively called mid-cycle (MC), whereas the phases one day before or after TO are called, respectively, late-cycle (LC) and early-cycle (EC).

2.2. Search for Botryllus MAPKs: in silico analyses, sequence alignment, and phylogenetic reconstruction

Two putative MAPK-encoding cDNA sequences from *B. schlosseri* were identified by searching the Octopus (https://octopus.obs-vlfr.fr/blast/botrylle/blast_botryllus.php) and ANISEED (https://www.aniseed.fr/) databases. The two sequences showed 85.8% and 69.9% identity to the human ERK-2 and JNK-1 cDNAs, respectively, and are hereafter referred to as *bsmapk-1* and *bsmapk-8*. Following PCR amplification and sequencing (see below; primers are listed in Table S1), the identities of the characterised sequences were confirmed by BLAST analysis against the NCBI database (https://blast.ncbi.nlm.nih.gov/Blast.cgi), and the resulting partial transcript sequences were deposited in GenBank (see below). Full-length transcripts were subsequently reconstructed *in silico* based on fully matching entries from the ANISEED and Octopus databases. The predicted protein sequences were obtained using the ExPASy translation tool (https://web.expasy.org/translate/) and analysed for conserved domain architecture with the SMART database (https://smart.embl.de/).

For domain-level comparisons, BsMAPK-1 and BsMAPK-8 were aligned with orthologous MAPK proteins from other metazoans retrieved from the NCBI database using the Clustal Omega multiple sequence alignment program (https://www.ebi.ac.uk/jdispatcher/msa/clustalo; NCBI accession numbers are reported in Tables S2 and S3). Pairwise identity and similarity values were calculated using the LALIGN tool (https://www.ebi.ac.uk/jdispatcher/psa/lalign). In addition, site-specific selective pressures acting on the protein sequences were further evaluated using the Selecton software (http://selecton.tau.ac.il/).

Phylogenetic analyses were conducted on MAPK-1 and MAPK-8 amino acid sequences from metazoans previously used for domain analysis, together with additional MAPK sequences retrieved from the NCBI database corresponding to MAPK-3, MAPK-9, MAPK-10, and MAPK-14 (Tables S2–S4). These sequences represent the major isoforms of the three principal classes of MAPKs. Full-length protein sequences were aligned using the Multiple Sequence Comparison by Log-Expectation (MUSCLE) algorithm. The resulting alignment was used to determine the best-fitting amino acid substitution model with the Molecular Evolutionary Genetics Analysis X (MEGA X) software. Phylogenetic relationships were inferred using the Bayesian Inference method implemented in MrBayes v3.2.7a. Four independent runs were performed, each consisting of four simultaneous Markov Chain Monte Carlo (MCMC) chains, for a total of 100,000,000 generations, with trees sampled every 1000 generations. Annotated phylogenetic trees were visualised using FigTree v1.4.4.

2.3. Primers, antibodies and inhibitors

Primers for quantitative real-time PCR (qRT-PCR) (Table S1) were designed on the partial coding DNA sequence (CDS) of the characterised sequences. Primer parameters (melting temperature, GC content, hairpin, self-dimer, and heterodimer) were checked using the IDT Oligo Analyzer (https://eu.idtdna.com/calc/analyzer), and primers were subsequently synthesized by Merck Life Science S.r.l. (Milan, Italy).

Polyclonal anti-human phospho-ERK-1/2 (anti-pERK) and polyclonal anti-human phospho-SAPK/JNK (anti-pJNK) primary antibodies were purchased from Cell Signalling Technology (Danvers, MA; catalogue numbers 9101 and 9251, respectively), and their specificity for the target proteins was previously validated by immunoblotting [47]. A polyclonal antibody raised against *Ciona robusta* TIAR (Bio-Fab Research S.r.l., Italy) was also used; its specificity in *B. schlosseri* has been previously demonstrated by immunoblot analysis [55]. The HRP-conjugated goat anti-rabbit IgG secondary antibody was purchased from Bio-Rad Laboratories (Hercules, CA, USA; catalogue number 1706515).

The inhibitors PD98059 and SP600125 were purchased from Sigma–Aldrich (St. Louis, MO) and were diluted in DMSO to a concentration of 100 mM (stock solutions).

2.4. Microinjections in B. schlosseri colonies

For intravascular microinjections of the solutions described below (1 μl every six zooids), peripheral ampullae (blind endings of the circulatory system) were punctured with thin glass capillaries, stretched with a Narishige puller, inserted into a PLI-100 pico-injector (Medical Systems Corp, Greenvale, NY). The efficacy of the injection was monitored under a stereomicroscope, as all solutions contained 0.025% phenol red.

For inhibitor treatments, colonies at MC were divided into subclones and microinjected with either PD98059 (ERK inhibitor, 100 μM in FSW), SP600125 (JNK inhibitor, 100 μM in FSW), or FSW containing 0.1% DMSO (reference control), the last concentration corresponding to the solvent concentration in the inhibitor working solutions. The concentrations of the inhibitors were considered sub-lethal, as they did not increase haemocyte mortality *in vitro* [47].

In another series of experiments, LPS (from *Escherichia coli* O55:B5; Sigma-Aldrich) was injected into colonies at MC at a final concentration of 1 mg/ml in FSW, a concentration known to trigger innate immune responses in *B. schlosseri* [61]. The following experimental groups were considered: 0 (reference control), 2, 4, and 6 h after LPS injection.

2.5. Protein extraction, electrophoresis and immunoblotting

Colonies were injected with FSW without (reference control) or with MAPK inhibitors at the concentrations reported above. One day after injection, samples were homogenised in ice-cold denaturing lysis buffer (50 mM Tris–HCl, pH 7.8, 25 mM sucrose, 5 mM EDTA, 2 mM sodium orthovanadate, 10 mM sodium fluoride, 5 mM N-ethylmaleimide, 1% SDS, 1 mg/mL pepstatin, 1 mg/mL leupeptin). Homogenisation was performed by mechanical disruption followed by sonication on ice (Bandelin Sonopuls sonifier; 50% duty cycle, three 20 s pulses with 10 s intervals). Lysates were centrifuged at 12,000 × g for 15 min at 4 °C, and supernatants were collected.

Protein concentration was determined using the Bradford assay [62]. Aliquots containing 20 μg of total protein were mixed with Laemmli sample buffer (0.5 M Tris–HCl, pH 6.8, 10% SDS, 10% glycerol, 5% β-mercaptoethanol, 0.05% bromophenol blue), heated at 95 °C for 7 min to ensure protein denaturation, and separated by SDS–PAGE on 12% polyacrylamide gels [63]. Electrophoresis was performed at a constant voltage of 80 V. Proteins were transferred onto nitrocellulose membranes (0.2 μm Hybond-ECL, GE Healthcare) using a Bio-Rad Trans-Blot semi-dry system with transfer buffer (25 mM Tris, 160 mM glycine, 20% methanol, 0.02% SDS).

Membranes were blocked for 2 h at room temperature in TBST (20 mM Tris–HCl, 150 mM NaCl, 0.1% Tween-20, pH 7.6) containing 3% normal goat serum and 2% bovine serum albumin. Membranes were then incubated overnight at 4 °C with primary antibodies (anti-pERK or anti-pJNK, 10 μg/mL; or anti-TIAR, 2 μg/mL), applied on separate membranes. After washing in TBST, membranes were incubated for 2 h

at room temperature with horseradish peroxidase (HRP)-conjugated secondary antibody (1:5000). Immunoreactive bands were detected using 0.025% 3,3′-diaminobenzidine (DAB) in TBST, containing 0.0125% hydrogen peroxide, for 10 min. In the presence of HRP, DAB is oxidised by hydrogen peroxide, resulting in the formation of an insoluble brown precipitate at the site of antibody binding.

Membranes were imaged and band intensity was quantified using ImageJ software (NIH). Integrated density values were calculated after background subtraction.

2.6. RNA sample preparation

The transcriptional activity of *bsmapk-1* and *bsmapk-8* was evaluated throughout the blastogenetic cycle. For this purpose, colonies of *B. schlosseri* at the EC, MC, LC, and TO phases were frozen in liquid nitrogen and stored at −80 °C until RNA extraction. The MC phase was chosen as a reference control because it is well away from the extensive apoptotic events that characterise the TO phase, when the cells of the old zooid generation undergo cell death and are cleared by circulating phagocytes infiltrating into the tissues and engulfing them [58].

To study the modulation of MAPK genes in response to immune stimulation, colonies at the MC were microinjected with LPS (1 mg/ml in FSW), frozen in liquid nitrogen after 0 (reference control), 2, 4, or 6 h, then stored at −80 °C until processing.

In another series of experiments, MC colonies were microinjected with the previously described inhibitors dissolved in FSW, or FSW containing 0.1% DMSO (reference control), and after 24 h, they were frozen in liquid nitrogen and stored at −80 °C. Colonies at this phase have been reported to display the highest transcription levels of antioxidant-related genes, such as *bssod* and *bsgpx-5* [51], as well as SG-related genes, including *bstiar* and *bsttp* [55,56]. Therefore, the transcription of these genes, together with that of MAPK genes, was quantified to investigate the potential involvement of MAPK pathways in their regulation.

To evaluate the effects of metals on MAPK gene transcriptions, colonies at MC were incubated in FSW containing 0.2 μM $CuCl_2$, $ZnCl_2$, or $CdCl_2$ (two essential and one non-essential metal, respectively), for 0 (reference control), 2, 4, or 6 h. Previous experiments indicated that these sub-lethal concentrations of metals were effective in inducing oxidative stress [51]. Metal stock solutions were prepared by dissolving the respective salts in distilled water, and their concentrations were verified using a PerkinElmer 4000 atomic absorption spectrophotometer. After treatments, colonies were frozen in liquid nitrogen and stored at −80 °C.

2.7. Total RNA extraction, cDNA synthesis, amplification, and sequencing

Total RNA was isolated by the precipitation method, using cetyltrimethylammonium bromide (CTAB, PanReac AppliChem) and PRIMeZOL (Canvax), combined in a 1:1 ratio, as lysis buffer, with the addition of 0.04% β-mercaptoethanol [49]. Samples were incubated in the lysis buffer at 65 °C for 1 h after mechanical disruption. One volume of chloroform was then added, and samples were centrifuged (4 °C; 15 min at 12000 x g). One volume of isopropanol was added to the supernatants, and samples were incubated overnight at −20 °C for RNA precipitation. After centrifugation (4 °C; 10 min at 12000 x g), the pellets were washed twice with 80% ethanol and centrifuged again (4 °C; 5 min at 7500 x g). Finally, the pellets were air-dried and resuspended in nuclease-free water. Further purification of all RNA samples was performed with the RQ1 RNase-Free DNase (Promega) kit to remove any possible genomic contamination. RNA concentration and purity were assessed using the Nanodrop ND-1000 spectrophotometer (ThermoFisher Scientific), by checking the $A_{260/280}$ and $A_{260/230}$ ratios; RNA integrity was verified through the visualisation of ribosomal RNA bands on 1% agarose gel.

Reverse transcription, from 1 μg of each extracted total RNA, was performed using the BiotechRabbit cDNA Synthesis Kit, which includes Oligo (dT) primer for the selection of poly(A) tailed mRNA. The quality of the obtained cDNAs was checked by qualitative PCR, performed with 2X YourTaq PCR Master Mix (BiotechRabbit) kit and the primers for elongation factor (*bsef,* endogenous control), reported in Table S1, on a SimpliAmp Thermal Cycler (Applied Biosystems). For *bsmapk-1* and *bsmapk-8*, the obtained PCR fragments were isolated from 1.5% agarose gel with the Wizard SV Gel and PCR Clean-Up System (Promega) kit and sequenced by Eurofins genomics (Europe Shared Services GmbH, Ebersberg, Germany), to obtain the coding sequences for qRT-PCR primer design. Checked cDNAs were used for gene quantification by qRT-PCR.

2.8. Quantitative real-time PCR (qRT-PCR)

qRT-PCR was performed to evaluate the changes in transcript levels of *bsmapk-1*, *bsmapk-8*, *bssod*, *bsgpx-5*, *bstiar*, *bsttp* and *B. schlosseri* elongation factor (*bsef*), the latter used as the housekeeping gene, in the various experimental conditions described above. The qPCRBIO SyGreen Blue Mix Separate-ROX (PCR Biosystems, Wayne, PA, USA) kit was used, after adjusting ROX (quencher) concentration at 100 nM in a 10 μl volume reaction, containing <100 ng of cDNA and 0.2 μM of the primers listed in Table S1. The cycle parameters were set as follows: 95 °C for 2 min (denaturation), 38 cycles at 95 °C for 20 s and 60 °C for 1 min (annealing), followed by a melting curve step (95 °C for 15 s, 60 °C for 1 min, 95 °C for 15 s, and 60 °C for 15 s). Each cDNA was analysed in triplicate, and the melting profile was used to verify the absence of genomic contamination. Relative expression levels were calculated with the $2^{-\Delta\Delta Ct}$ method [64]. Transcription levels were normalised to the housekeeping gene, to compensate for variations in the amounts of cDNA.

2.9. Collection of haemocytes

The tunic marginal vessel of colonies at MC, previously rinsed in 0.38% Na-citrate in FSW, pH 7.5, to prevent haemocyte clotting, was punctured with a fine tungsten needle and flowing haemolymph was collected with a glass micropipette. It was centrifuged at 780 x g for 10 min and the pellet was resuspended in FSW to obtain a final concentration of 5 x 10^5 cells/ml. Sixty μl of haemocyte suspension was placed in the centre of culture chambers prepared as described elsewhere [65]; they were kept upside-down for 30 min to allow the adhesion of haemocytes to coverslips. Cell viability was evaluated with the Trypan blue exclusion assay. Briefly, cells were incubated in a solution of 0.25% Trypan blue in FSW for 5 min and then observed under the light microscope; the frequency of blue (=dead) cells was finally evaluated.

2.10. Immunocytochemical analysis

Haemocytes were incubated for 60 min with either FSW (control) or yeast (*Saccharomyces cerevisiae*)-containing FSW (yeast:haemocyte ratio = 10:1), in the presence or absence of inhibitors at the concentration of 10 μM, according to *in vitro* analyses carried out by Franchi et al. [47], and subsequently washed in FSW and fixed for 30 min at 4 °C in 4% paraformaldehyde plus 0.1% glutaraldehyde in 0.2 M Na-cacodylate buffer (pH 7.4) containing 1.7% NaCl and 1% sucrose, rinsed in phosphate-buffered saline (PBS: 1.37 M NaCl, 0.03 M KCl, 0.015 M KH_2PO_4, 0.065 M Na_2HPO_4, pH 7.4). After washing in PBS, haemocytes were permeabilised with 0.1% Triton X-100 in PBS for 5 min, washed again in PBS and treated for 30 min with a solution of 6% H_2O_2 in methanol to block endogenous peroxidase activity. Before antibody incubation, haemocytes were washed in PBS and blocked with 5% normal goat serum in PBS for 30 min to prevent non-specific binding. Polyclonal anti-pERK or anti-pJNK primary antibodies were diluted

in blocking solution (1:200) and applied overnight at 4 °C. After washing in PBS, haemocytes were incubated with HRP-conjugated secondary antibody diluted in blocking solution (1:500) for 2 h at room temperature. Detection was performed using 0.025% DAB in PBS, in presence of 0.0125% hydrogen peroxide, for 10 min. Coverslips were finally mounted in Acquovitrex (Carlo Erba, Italy). Cells were observed under a light microscope and the fraction of immunopositive cells was evaluated.

2.11. Phagocytosis assay

Haemocytes from colonies at MC were exposed for 30 min to the inhibitors described above (10 μM in FSW). They were then washed in FSW and incubated with 60 μl of a suspension of yeast (yeast:haemocyte ratio = 10:1). Cultures were kept inverted for 60 min, and, at the end of the incubation period, coverslips were repeatedly dipped into a large volume of FSW to remove unattached yeast. Haemocytes were then fixed, as previously described, and stained with 10% Giemsa for 10 min, and the coverslips were mounted as previously described. About 200 cells per slide, in ten optic fields at the magnification of 1250×, were observed under a light microscope and the percentage of haemocytes containing ingested yeast cells was calculated.

2.12. Effects on the blastogenetic cycle

To investigate the effects of MAPK inhibition on colony development during the blastogenetic cycle, three large colonies were divided into subclones of at least three systems. Daily injections began on the second day after TO. Digital images of the subclones were acquired daily before each injection, and the area of adult zooids was measured using ImageJ software. Measurements obtained from treated subclones were compared with those from the corresponding control subclones derived from the same parental colony.

2.13. Statistical analysis

For morphological analyses, three independent colonies (n = 3) were used. From each colony, one control subclone and two inhibitor-treated subclones were analysed, and at least 6 zooids per subclone were measured. Areas of zooids were expressed as means ± standard deviations.

Relative values obtained by qRT-PCR were expressed as means ± standard deviations of three independent colonies (n = 3). Data distribution was assessed using the Shapiro–Wilk test. Differences among groups were evaluated by one-way analysis of variance (ANOVA), followed by Tukey's post hoc test for multiple comparisons. Differences were considered statistically significant at $p < 0.05$.

Immunocytochemical and phagocytosis assays were carried out using cells from three independent colonies (n = 3). Data were compared using the chi-square (χ^2) test.

3. Results

3.1. Amplification and partial characterisation of bsmapk-1 and bsmapk-8

The PCR fragment amplified with the BsMAPK-1Fw and BsMAPK-1Rv primers and with the BsMAPK-8Fw and BsMAPK-8Rv primers, once sequenced, allowed us to characterise part of the CDS of two MAPK genes. Both, the first one 727 nucleotides long and the second one 883 nucleotides long, correspond to the putative sequences found in the ANISEED database (transcript ID: Boschl.CG.Botznik2013.chrUn.g60494.01.t and Boschl.CG.Botznik2013.chr7.g45587.01.t, respectively). These results confirm that the genes are transcribed in *B. schlosseri*. The first PCR fragment showed a high similarity (95.0%) and identity (78.3%; *E*-value: 3e-157) with the *mapk-1* sequence of *Fundulus heteroclitus* (NCBI accession number XM_036144364.1) and was named *bsmapk-1*. The second PCR fragment showed the highest similarity (99.0%) and identity (75.6%; *E*-value: 2e-172) with the *mapk-8* sequence of *Styela clava* (NCBI accession number XM_039397647.2) and was named *bsmapk-8*. The *in silico* reconstruction of the first transcript resulted in a full-length sequence of 2418 nucleotides, with 5′-UTR and 3′-UTR regions of 48 and 1278 nucleotides, respectively, with a CDS of 1092 nucleotides, encoding a putative protein of 364 amino acids with a deduced molecular weight of 42 kDa (Fig. S1). For the second transcript, a full-length sequence of 1980 nucleotides was obtained, with 5′-UTR and 3′-UTR regions of 249 and 462 nucleotides, respectively, and a CDS of 1269 nucleotides, encoding a putative protein of 423 amino acids with a deduced molecular weight of 47.4 kDa (Fig. S2). The partial transcript sequences were deposited in GenBank under the following accession numbers: PX411264.1 for *bsmapk*-1 and PX411265.1 for *bsmapk*-8.

3.2. Domain architecture and phylogenetic validation of BsMAPK-1 and BsMAPK-8

The reconstructed amino acid sequence of BsMAPK-1 (Fig. S1) showed the highest similarity (98%) and identity (87.1%) to the MAPK-1 sequence of *S. clava* (NCBI accession number XP_039266663.1), whereas the reconstructed amino acid sequence of BsMAPK-8 (Fig. S2) showed the highest similarity (97%) and identity (85.1%) to the MAPK-8 sequence of *S. clava* (NCBI accession number XP_039253581.2). Multiple alignment of the sequences revealed that the serine/threonine catalytic domains are highly conserved (75.4% and 66.7% of identical residues, respectively). Within this domain, the catalytic sites, represented by the threonine-glutamate-tyrosine (TEY) and the threonine-proline-tyrosine (TPY) motifs, respectively, are fully conserved across all analysed species (100% identity) (Figs. S3 and S4). Selection analysis of the two sequences (Figs. S5 and S6) indicates that purifying selection predominates, affecting 80.7% and 78.9% of residues, respectively. The degrees of identity and similarity resulting from comparison of BsMAPK-1 and BsMAPK-8 with orthologous metazoan sequences, obtained using the LALIGN tool, are reported in Tables S2 and S3, respectively.

The MEGA X software identified the LG + G model as the best-fit substitution model for analysing the evolution of MAPK amino acid sequences, with a gamma shape parameter of 0.52 (four rate categories), based on the corrected Akaike Information Criterion (cAIC) and Bayesian Information Criterion (BIC) (-InL = 10662.745). The phylogenetic tree inferred using the Bayesian Inference method (Fig. S7) is fully resolved, with all nodes supported by Bayesian posterior probabilities ranging from 61% to 100%. The clade comprising ascidian sequences, including *B. schlosseri* and *S. clava*, is strongly supported (100% posterior probability) and is recovered as a sister group to vertebrate sequences for MAPK-1, and to invertebrate sequences for MAPK-8.

3.3. The transcriptional activity of bsmapk-1 and bsmapk-8 is modulated during the colonial blastogenetic cycle

During the blastogenetic cycle, *bsmapk-1* transcription levels showed limited fluctuations, with a significant ($p < 0.05$) increase at the TO phase, corresponding to a 7.8-fold increase relative to MC (third day post-TO, reference value) (Fig. 1A). In contrast, *bsmapk-8* expression reached its highest level at LC, significantly ($p < 0.01$) different from the levels observed during the first three days post-TO and corresponding to a 45.2% increase relative to the reference value. Conversely, the lowest level was recorded one day after EC, corresponding to a 17.5% decrease compared to the MC reference (Fig. 1B).

3.4. Immunoblot analysis reveals the inhibition of MAPKs by MAPK inhibitors

Colony lysates, previously injected with FSW (control) or with MAPK

1	2	3	4	5	6-7	days post-TO
	0.016	**0.016**	**0.006**	**0.038**	**0.017**	1
		0.060	**0.044**	0.346	**0.020**	2
			0.586	0.251	**0.024**	3
				0.375	**0.023**	4
					0.021	5

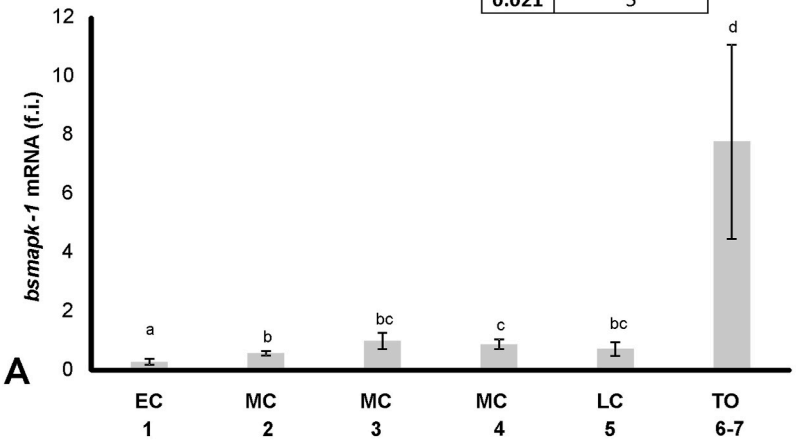

1	2	3	4	5	6-7	days post-TO
	0.279	0.057	0.112	**0.006**	0.145	1
		0.067	0.066	**0.006**	0.100	2
			0.274	**0.009**	0.215	3
				0.068	0.430	4
					0.675	5

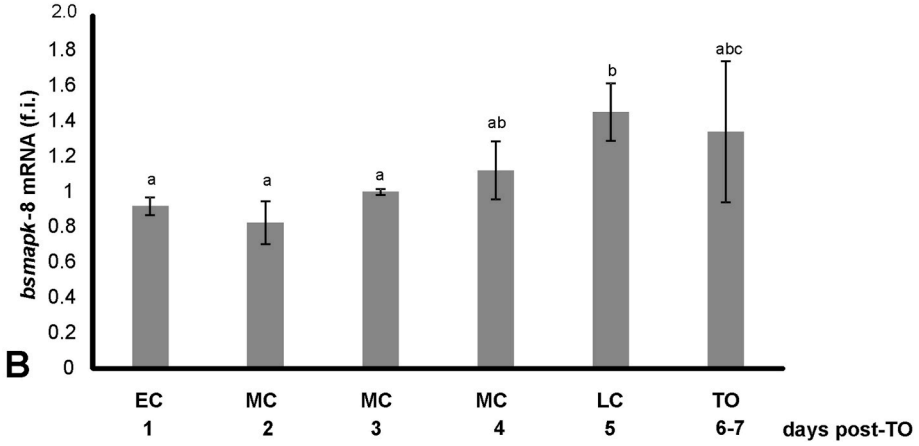

Fig. 1. Relative transcriptional activity (fold induction, f.i.) of *bsmapk-1* (A) and *bsmapk-8* (B) during the blastogenetic cycle of *B. schlosseri*. EC: early-cycle; MC: mid-cycle; LC: late-cycle; TO: take-over. Values were compared with the MC transcription level at third day of the cycle (relative value = 1). Different letters denote statistically significant differences among days within the blastogenetic cycle ($p < 0.05$). *p*-values for the comparisons are reported in the table above the graphs. Significant differences are indicated in bold. The degrees of freedom were 4 for all comparisons.

inhibitors, contained proteins recognised by anti-pERK and anti-pJNK antibodies. In the immunoblot analysis, the anti-pERK antibody identified two bands of 42 and 44 kDa (Fig. 2A), whereas the anti-pJNK antibody recognised a single band of 46 kDa (Fig. 2B). Band intensity was markedly reduced in the presence of the MAPK inhibitors. In particular, PD98059 reduced the intensity of the bands detected by the anti-pERK antibody to 13% of the control band intensity, whereas SP600125 reduced the intensity of the 46-kDa band to 17.6% of the control band intensity (Fig. 2A and B).

3.5. Transcriptional effects of MAPK inhibitors

In colonies injected with PD98059, no significant effects on the transcription levels of either *bsmapk-1* or *bsmapk-8* were observed compared with the controls. Conversely, treatment with SP600125 significantly ($p < 0.05$) reduced the transcription levels of *bsmapk-1* and *bsmapk*-8 by 73.5% and 63.6%, respectively, relative to the controls (Fig. 3A).

As for SG-related genes, the injection of PD98059 significantly ($p < 0.001$) reduced the transcription of *bstiar* and *bsttp* by 45.5% and 75.7%, respectively, whereas SP600125 significantly ($p < 0.001$) induced a 13.15-fold increase in *bstiar* transcription (Fig. 3B). This result

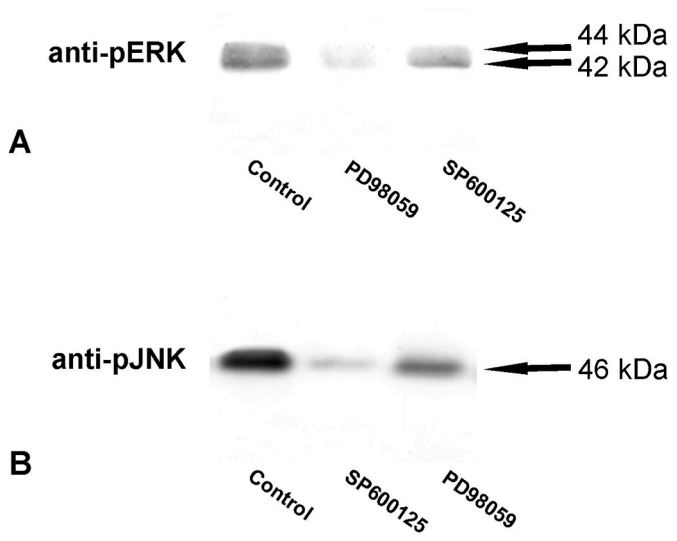

Fig. 2. Immunoblot analysis of proteins recognised by anti-pERK (A) and anti-pJNK (B) antibodies in lysates from control colonies and colonies treated with the inhibitors PD98059 and SP600125.

mirrored what was obtained in the immunoblot analysis with the anti-TIAR antibody: the 50-kDa band was more intense (60.5% increase) than the control band in SP600125-injected colonies and markedly less intense (78% decrease) in colonies treated with PD98059 (Fig. S8).

Regarding other stress-related genes, the injection of PD98059 caused a significant ($p < 0.01$) reduction of *bssod* and *bsgpx-5* transcription relative to the controls by 84.8% and 45.6%, respectively, whereas SP600125 led to a significant ($p < 0.01$) decrease in *bssod* and *bsgpx-5* transcriptional activity by 96.0% and 49.2%, respectively, relative to the controls (Fig. 3C).

3.6. The MAPK inhibitors impair B. schlosseri phagocytosis

To confirm the inhibitory effects of PD98059 and SP600125 on phagocytosis, haemocytes from *Botryllus* colonies were challenged with yeast to induce MAPK activation in phagocytes, as previously demonstrated by Franchi et al. [47], using zymosan as a non-self stimulus. The Trypan Blue assay indicated that more than 95% of the cells were viable after haemolymph collection.

Control haemocytes, not challenged with yeast, did not show any labelling with the anti-pERK antibody (Fig. 4A) or anti-pJNK antibody; in contrast, round phagocytes containing ingested yeast cells were strongly labelled with the anti-pERK (Fig. 4B) or anti-pJNK antibody (Fig. 4C). Pre-incubation with PD98059 (Fig. 4D) or SP600125, in the presence of yeast, markedly reduced both the intensity of immunopositivity and the number of immunopositive cells compared with the yeast-challenged controls ($p < 0.001$; Fig. 4E).

Phagocytosis of yeast cells was significantly ($p < 0.05$) reduced following pre-incubation with either PD98059 or SP600125. The fraction of phagocytes ingesting yeast decreased to 35% and 80% of the control value for PD98059 and SP600125, respectively (Fig. S9).

3.7. The transcription of bsmapk-1 and bsmapk-8 is modulated by LPS

In LPS-microinjected colonies, variations in *bsmapk-1* and *bsmapk-8* transcript levels were observed. Two h after LPS injection, *bsmapk-1* transcription did not differ from the control. At 4 h, it became significantly ($p < 0.05$) higher, reaching almost three-fold increase relative to the control, and at 6 h it was significantly ($p < 0.01$) reduced by 83% relative to the control. Conversely, *bsmapk-8* transcription gradually increased from 2 to 6 h, remaining significantly ($p < 0.05$) higher than the control at all time points analysed, and reaching a maximum 18.8-fold increase relative to the control at 6 h post-injection (Fig. 5).

3.8. Metals modulate the transcription of B. schlosseri MAPK genes

Previous studies have shown that metals can influence the transcription of ascidian genes [66–68]. In our experiments, exposure to Cu^{2+} induced a significant ($p < 0.05$) decrease in *bsmapk-1* transcription at 2 h and 4 h compared with the control, followed by significant ($p < 0.001$) increase after 6 h, reaching approximately 7.8-fold the control value. In contrast, *bsmapk-8* showed a complex response to Cu^{2+}. At 2 h, its transcription was significantly ($p < 0.001$) downregulated, with a 92.6% reduction relative to the control. At 4 h, a significant ($p < 0.001$) upregulation was observed, with a 6.4-fold increase relative to the control. At 6 h, transcription was strongly downregulated ($p < 0.001$), with a 99.7% reduction relative to the control (Fig. 6A).

Similarly, Zn^{2+} exposure caused a significant ($p < 0.05$) decrease of *bsmapk-1* transcription, at 4 h compared with the control, and a significant ($p < 0.001$) 11.1-fold increase at 6 h. As regards *bsmapk-8*, transcription was significantly ($p < 0.01$) downregulated at 2 h and 4 h, and showed no significant changes at 6 h, relative to the control (Fig. 6B).

Regarding Cd^{2+}, *bsmapk-1* transcription showed a significant ($p < 0.001$) reduction at 2 h with respect to the control but was significantly ($p < 0.05$) upregulated at 6 h, with a 3.8-fold increase relative to control. Conversely, *bsmapk-8* displayed a significant ($p < 0.01$) upregulation at 2 h (4.8-fold relative to the control), followed by significant ($p < 0.01$) downregulation at 4 h and 6 h (68.4% and 97.5% reduction relative to the control, respectively) (Fig. 6C).

3.9. Effect of MAPK inhibitors on the colonial blastogenetic cycle

Phagocytes are essential for the clearance of effete cells and for the progression of the blastogenetic cycle [57]. To assess the role of MAPK signalling in these processes, we examined the effects of prolonged exposure to the above inhibitors on *B. schlosseri* colonies. Treatment with PD98059 induced a significant ($p < 0.05$) reduction in zooid size compared with the controls as early as day 1, and this difference progressively increased until day 5, when TO occurred one day earlier than in the control colonies (Fig. 7A). At this time point, the area of treated zooids was reduced by 77.4% relative to the control. During the final two days of the experiment, the new generation of treated zooids remained markedly ($p < 0.001$) smaller than controls, reaching by day 9 an average area 56.2% lower than that of the control. At day 9, when the control colony was in MC (images not shown), the treated colony (Fig. 7B) displayed a reduction in number of zooid from nine to six. The remaining zooids were in an advanced phase of resorption, characterised by closed siphons, absence of developing buds, and surrounding vessels filled with dark haemolymph cells.

Significant ($p < 0.05$) differences between SP600125-treated and untreated colonies were first observed on day 1 (Fig. 8A). From day 3 onward, treated zooids remained consistently smaller than controls ($p < 0.001$). The TO occurred on day 5 in both groups; however, treated zooids were significantly ($p < 0.001$) reduced in size, approximately 57.5% smaller than the control. This difference persisted through day 9, when treated zooids still exhibited significantly ($p < 0.001$) smaller areas, corresponding to about 21.8% smaller than the control. On days 8 and 9, the treated colony (Fig. 8B) failed to progress through the blastogenetic cycle, with its zooids arrested in MC. In the treated colony, a zooid was lost following TO, and the remaining nine appeared slightly malformed and lacked developing budlets.

4. Discussion

In the present study, by mining two transcriptomic databases of *B. schlosseri* (ANISEED and Octopus), we identified and characterised two MAPK transcripts showing high similarity to chordate MAPK-1 (ERK-2) and MAPK-8 (JNK-1), which we designated as BsMAPK-1 and

bsmapk-1		*bsmapk-8*	
comparison	*p*-value	comparison	*p*-value
C *vs* PD98059	0.06	C *vs* PD98059	0.054
C *vs* SP600125	**0.039**	C *vs* SP600125	**0.022**

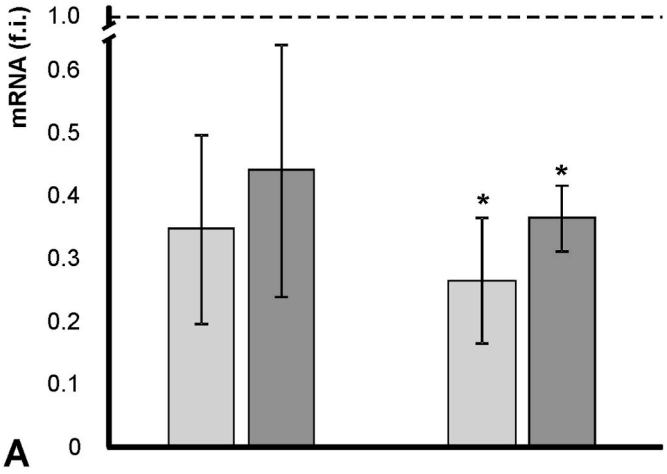

bstiar		*bsttp*	
comparison	*p*-value	comparison	*p*-value
C *vs* PD98059	**< 0.001**	C *vs* PD98059	**< 0.001**
C *vs* SP600125	**< 0.001**	C vs SP600125	0.092

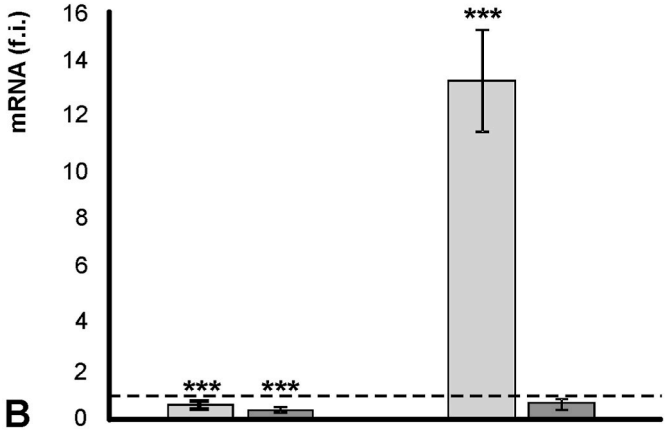

bssod		*bsgpx-5*	
comparison	*p*-value	comparison	*p*-value
C *vs* PD98059	**< 0.001**	C *vs* PD98059	**0.002**
C *vs* SP600125	**< 0.001**	C vs SP600125	**0.002**

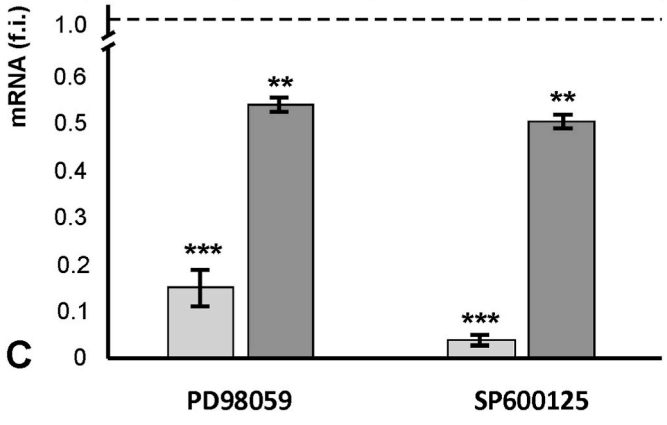

(caption on next column)

Fig. 3. Relative transcriptional activity (fold induction, f.i.) of *bsmapk-1* and *bsmapk-8* (A), *bstiar* and *bsttp* (SG-related genes) (B), *bssod* and *bsgpx-5* (oxidative stress-related genes) (C), in colonies of *B. schlosseri* 24 h after microinjections of the MAPK inhibitors PD98059 or SP600125. Values were compared with the reference transcription level (relative value = 1, dotted line), corresponding to that of control colonies (injected with FSW containing 0.1% DMSO). Asterisks indicate statistically significant differences relative to the controls (*: $p < 0.05$; **: $p < 0.01$; ***: $p < 0.001$). *p*-values for the comparisons are reported in the table above the graphs. Significant differences are indicated in bold. The degrees of freedom were 4 for all comparisons.

BsMAPK-8, respectively. Phylogenetic analysis of MAPK amino acid sequences from vertebrate and invertebrate species revealed a clear separation of the major MAPK subfamilies, including the ERK (MAPK-1/MAPK-3), JNK (MAPK-8/MAPK-9/MAPK-10), and p38 (MAPK-14) lineages. The two *B. schlosseri* sequences clustered within the MAPK-1 and MAPK-8 lineages, respectively, consistent with their high sequence similarity to vertebrate orthologues. This high similarity justifies the use of antibodies raised against mammalian proteins to detect ascidian ones. Indeed, the anti-pERK antibody recognised two bands of 42 and 44 kDa, likely corresponding to different phosphorylated forms of ERK-related proteins detected by the antibody, whereas the anti-pJNK antibody detected a single band of 46 kDa. On the basis of the phylogenetic conservation of these proteins, we ascribed the observed bands to BsMAPK-1 and BsMAPK-8, respectively, as their molecular weights are consistent with those reported for orthologous proteins in mammals. Notably, BsMAPK-1 and BsMAPK-8 showed the highest similarity to the corresponding proteins of *S. clava*, another ascidian species, highlighting the strong evolutionary conservation of these kinases within tunicates. In addition, *in silico* analyses of the translated amino acid sequences, compared with orthologous sequences from a broad range of metazoans, revealed complete conservation of the catalytic site in both kinases. This conservation underscores the strong evolutionary constraints acting on this domain, which is essential for MAPK signalling activity [69]. Consistent with this, selection analyses indicated that most amino acid residues in BsMAPK-1 and BsMAPK-8 are subject to purifying selection, limiting the accumulation of deleterious mutations and preserving protein structural and functional integrity.

We next analysed the transcriptional activity of both MAPK genes during the *Botryllus* blastogenetic cycle. *bsmapk-8* exhibited its highest transcription levels at the LC and TO phases, when most of the cells of the old zooid tissues undergo apoptosis and are removed by circulating phagocytes [58]. Given its high similarity to mammalian JNK, mainly involved in stress responses and innate immunity [9], we hypothesise that BsMAPK-8 activity may contribute to the regulation of phagocytosis, ensuring the clearance of effete cells and cellular debris. This regulation appears to be critical for the transition between generations, from bud and budlet stages to adult zooids, and for the removal of old zooids at TO [57]. As for *bsmapk-1*, its expression markedly increased at the TO. Since BsMAPK-1 shares similarity to mammalian ERK, a kinase involved in cell differentiation and proliferation [12], we propose that *bsmapk-1* plays a key role in sustaining the generation change, reaching its peak activity at TO, a phase characterised by intense proliferative processes required for bud growth and replacement of old haemocytes via the release of new circulating precursor cells [59]. The coexistence of extensive apoptosis and intense proliferative activity during TO suggests that MAPK pathways act as molecular switches coordinating the degeneration of the old generation with the development of the new one. These transcriptional patterns are consistent with the established functions of JNK and ERK pathways in metazoans [16,18,47].

Then, we studied the effects of the microinjection of the above-reported MAPK inhibitors in the colonial circulation. The microinjection of PD98059 and SP600125 reduced the intensity of the bands recognised by anti-pERK and anti-pJNK. PD98059 is an ERK-1/2 inhibitor as it prevents the phosphorylation of ERK by blocking the activation of the enzymes upstream of ERK-1/2 [70]; this mechanism is consistent

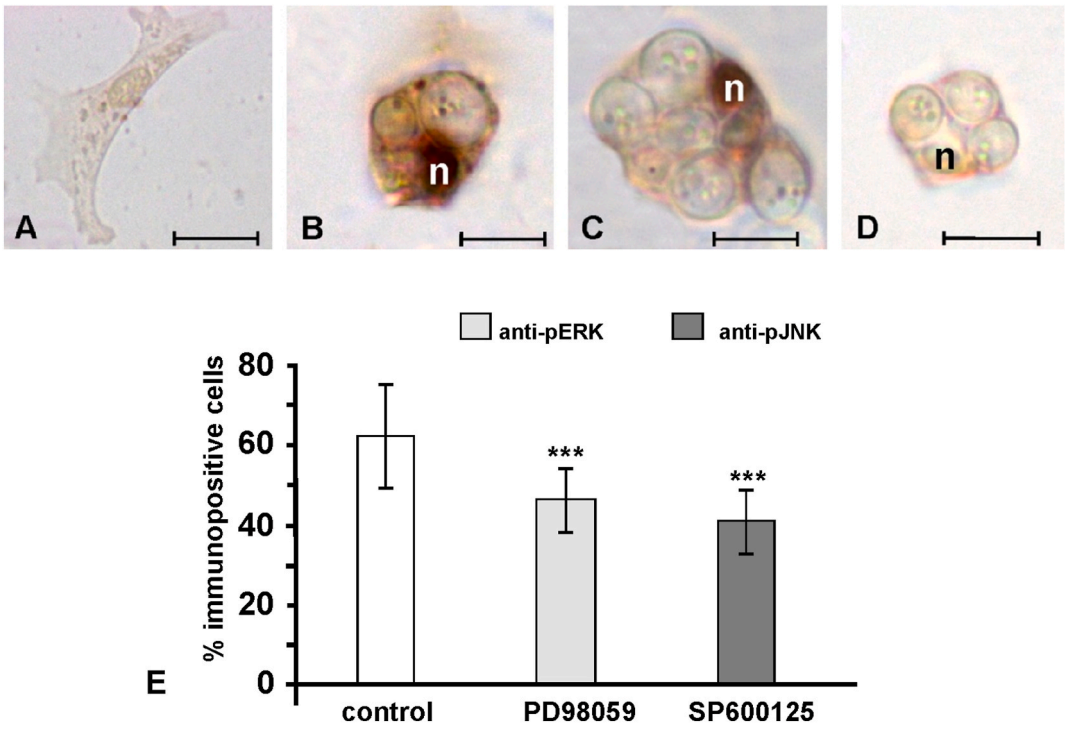

Fig. 4. Immunostaining of *B. schlosseri* phagocytes with anti-pERK (A, B, D) or anti-pJNK (C) antibodies, and fraction phagocytes immunopositive to anti-pERK or anti-pJNK antibodies following yeast challenge, in the presence or absence (controls) of the MAPK inhibitors PD98059 or SP600125 (E). (A) Spreading control phagocyte not challenged with yeast. (B–C) Round phagocytes challenged with yeast. (D) Round phagocyte treated with the MAPK inhibitor PD98059 during yeast challenge. n: nucleus. Scale bar: 10 μm. Asterisks indicate statistically significant differences compared with controls (***: $p < 0.001$).

bsmapk-1		*bsmapk-8*	
comparison	*p*-value	comparison	*p*-value
C *vs* 2	0.470	C *vs* 2	**0.029**
C *vs* 4	**0.038**	C *vs* 4	**0.002**
C *vs* 6	**0.006**	C *vs* 6	**< 0.001**

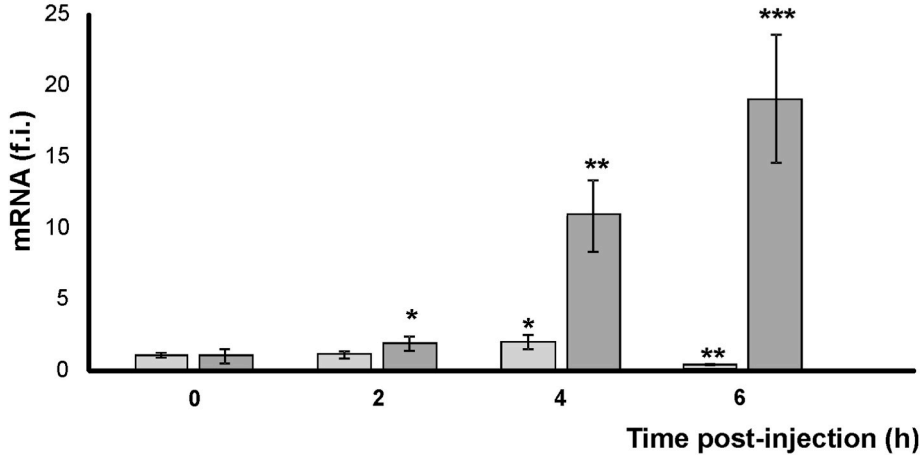

Fig. 5. Relative transcriptional activity (fold induction, f.i.) of *bsmapk-1* and *bsmapk-8* in colonies of *B. schlosseri* at 0 (reference control), 2, 4, and 6 h after LPS microinjection. Transcription levels are expressed relative to those of control colonies at time 0 (relative value = 1, dotted line). *p*-values for the comparisons are reported in the table above the graphs. Asterisks indicate statistically significant differences relative to the controls (*: $p < 0.05$; **: $p < 0.01$; ***: $p < 0.001$). Significant differences are indicated in bold. The degrees of freedom were 4 for all comparisons.

with the observed reduction of the intensity of the 42- and 44-kDa bands in our experiment. Conversely, SP600125 is a competitive JNK inhibitor preventing the downstream phosphorylation of c-Jun [71]. To explain the decrease in the intensity of the band ascribed to BsMAPK-8, we hypothesise that, analogously to what has been observed in mammals, where SP600125 can inhibit JNK phosphorylation as well [72–74], the same inhibitor also affects BsMAPK-8 activation/phosphorylation. The reported decrease in the intensity of the electrophoretic bands is also reflected, in colonies injected with the inhibitors, in the reduction of phagocyte staining by the anti-MAPK antibodies, a decrease in phagocytic activity of circulating haemocytes and the reduction of the fraction of circulating phagocytes immunopositive to anti-pERK and anti-pJNK

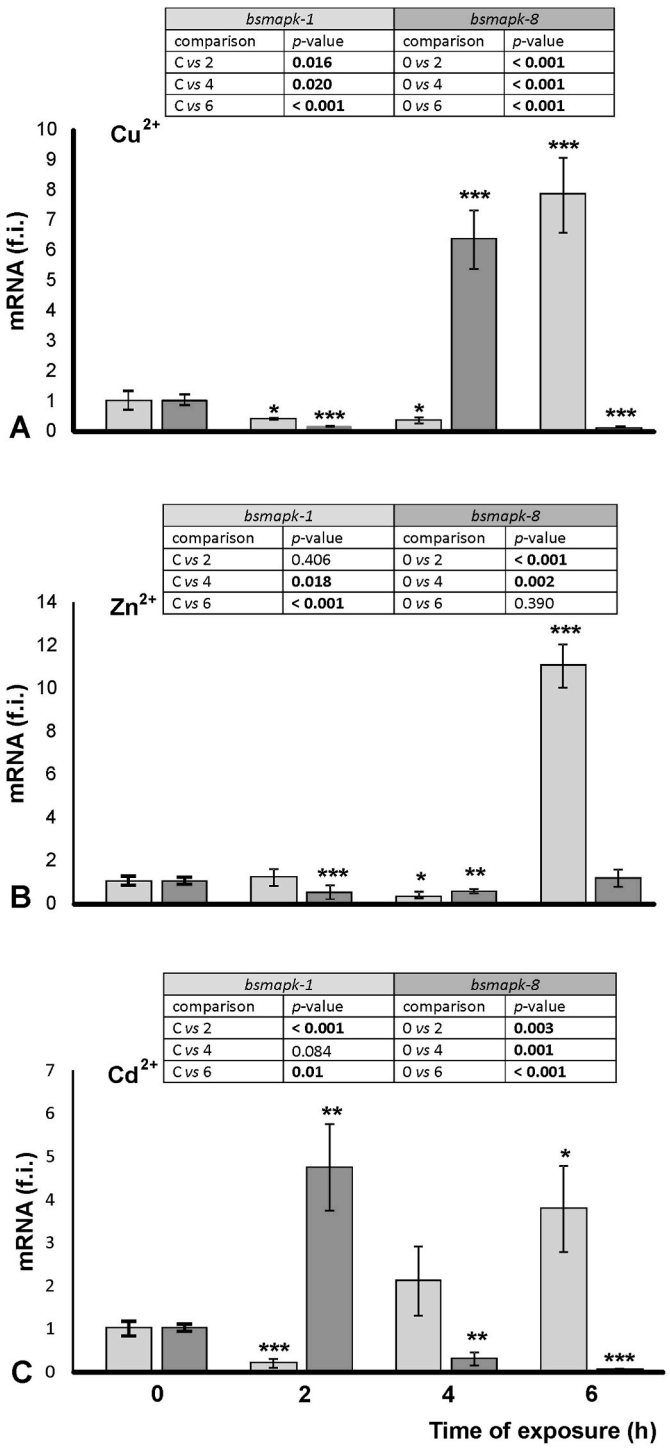

Fig. 6. Relative transcriptional activity (fold induction, f.i.) of *bsmapk-1* and *bsmapk-8* in colonies of *B. schlosseri* at 0 (reference control), 2, 4 or 6 h after exposure to Cu^{2+} (A), Zn^{2+} (B) or Cd^{2+} (C). Transcription levels are expressed relative to those of control colonies at time 0 (relative value = 1, dotted line). *p*-values for the comparisons are reported in the table above the graphs. Asterisks indicate statistically significant differences relative to the controls (*: $p < 0.05$; **: $p < 0.01$; ***: $p < 0.001$). Significant differences are indicated in bold. The degrees of freedom were 4 for all comparisons.

antibodies. All these observations point towards a significant role of *bsmapk-1* and *bsmapk-8* in the immune response of *B. schlosseri*.

Moreover, results showed a clear decrease in the transcription of both *bsmapk-1* and *bsmapk-8* following SP600125 treatment, whereas PD98059 had no significant effect. We assume that, by blocking the phosphorylation and activation of c-Jun, the activity of which is required to promote the transcription of various inflammatory and stress-related genes including the genes for MAPKs, SP600125 reduces the transcription of both *bsmapk-1* and *bsmapk-8*. The presence of such a feedback regulatory loop within the JNK–c-Jun signalling pathway has been reported in mammals [75,76]. In addition, although SP600125 primarily inhibits JNK activity, the observed decrease in *bsmapk-1* transcription suggests the possibility of additional regulatory interactions between the JNK and ERK pathways. This finding is consistent with previous reports describing JNK–ERK crosstalk in mammalian systems [77], suggesting that similar regulatory dynamics may also occurred in tunicates. However, as our analysis was limited to mRNA expression levels rather than kinase activity, additional assays will be necessary to determine whether the observed effect reflects direct pathway crosstalk or indirect transcriptional regulation mediated by downstream effectors and stress-responsive networks.

LPS challenge in *B. schlosseri* colonies altered the transcriptional profile of the analysed MAPK genes, in agreement with findings reported by Arizza et al. [54] in the solitary ascidian *C. robusta*. In mammalian cells, LPS triggers inflammation by activating MAPKs [78], which may also help explain the observed responses in our system. Notably, *bsmapk-8* transcription progressively increased, reaching its highest level at 6 h post-injection compared to control, suggesting a predominant involvement of BsMAPK-8 in the LPS-induced response and, consequently, a role of downstream JNK–c-Jun signalling, according to the hypothesis discussed before. In contrast, *bsmapk-1* transcription was only slightly elevated at 4 h, suggesting a more moderate or temporally restricted involvement, potentially also linked to JNK-dependent regulatory mechanisms or broader stress-responsive pathways.

MAPKs play a role also in stress responses [79–81], which include post-transcriptional regulatory mechanisms involving the formation of two distinct types of cytoplasmic complexes: stress granules (SGs) [82], and processing bodies (p-bodies) [83]. In SGs, selected mRNAs are temporarily stored and their translation is repressed [84], whereas in p-bodies, mRNAs no longer useful to the cell are degraded [85]. Among the mRNA-binding proteins (RBPs) involved in SG formation, TIA-1-related nucleolysin (TIAR) and tristetraprolin (TTP) can recognise and bind adenine/uridine (A/U)-rich elements in target mRNAs (e.g., cytokine mRNAs), through RNA recognition motifs (for TIAR) [86,87] or zinc-finger domains (for TTP) [88,89]. Given the known roles of mammalian MAPKs in immune and stress responses [16–18,90], we investigated the effects of the MAPK inhibitors on the transcription of genes involved in the formation of SGs. We observed that *bstiar* was upregulated by SP600125 injection. This is paralleled by the increase in the protein levels detected by the anti-TIAR antibody raised in ascidians [55]. In contrast, *bsttp* transcription was reduced upon PD98059 injection. We hypothesise that, like in mammals [91,92], the above-reported RNA-binding proteins serve as targets of MAPKs that phosphorylate them and regulate their ability to bind and stabilise target mRNAs. In agreement with the above assumption, in mouse and human cell lines, ERK mediates the phosphorylation of TTP thus protecting it from immediate proteasomal degradation [93]. Our results suggest that, in *B. schlosseri*, MAPKs may interact with genes encoding SG proteins and modulate their activity. In particular, *bstiar* appears to be regulated in association with JNK–c-Jun signalling, whereas *bsttp* may be functionally linked to MAPK-ERK signalling pathways.

Focusing on antioxidant proteins, the literature suggests a link between these proteins and MAPK signalling pathways. For instance, Mn-SOD is inhibited via JNK-dependent ubiquitination in human aortic endothelial cells [94]. Regarding GPXs, recent findings indicate that GPX-3 may be regulated by the JNK pathway, thereby affecting proliferation and migration of pancreatic cancer cells [95]. In our study, treatment with both MAPK inhibitors effectively suppressed the transcription of *bssod* and *bsgpx-5*, suggesting that both BsMAPK-1 and BsMAPK-8 may be involved in the regulation of genes associated with protection against oxidative stress. Consistently, both *bssod* and *bsgpx*-5

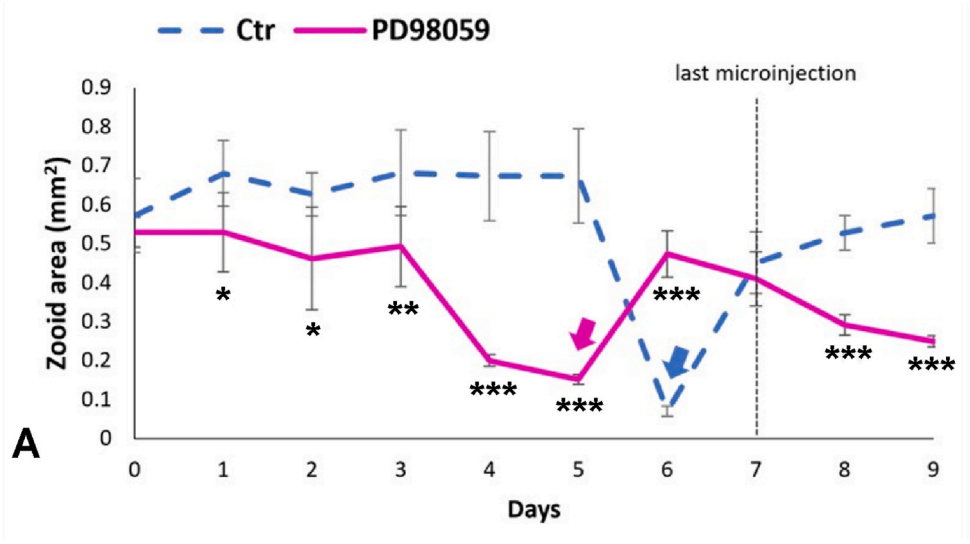

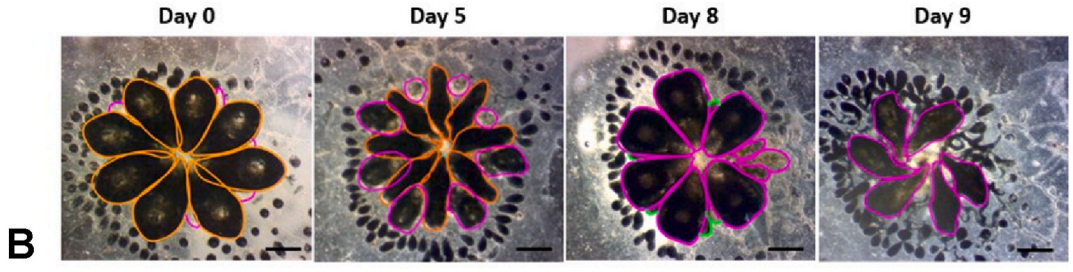

C

C vs treated		
day	*p*-value	degrees of freedom
0	0.274	12
1	**0.012**	12
2	**0.014**	12
3	**0.006**	12
4	**< 0.001**	12
5	**< 0.001**	9
6	**< 0.001**	10
7	0.391	12
8	**< 0.001**	12
9	**< 0.001**	12

Fig. 7. (A) Mean area of adult zooids in *B. schlosseri* colonies microinjected with PD98059 (solid line) or FSW containing 0.1% DMSO (control, dashed line) over a one-week experimental period. TO (indicated by arrows) occurred on day 5 in PD98059-treated colonies and on day 6 in control colonies. The final microinjection was administered on day 7. Asterisks indicate statistically significant differences between PD98059-treated and control colonies at the corresponding time points (*: $p < 0.05$; **: $p < 0.01$; ***: $p < 0.001$). (B) Representative colony treated with PD98059 and monitored throughout the experiment. Different colors identify successive zooid generations: orange (first generation), purple (second generation), and green (third generation). Scale bars = 0.5 mm. (C) Summary table of the statistical comparisons between control and PD98059-treated colonies. (For interpretation of the references to color in this figure legend, the reader is referred to the Web version of this article.)

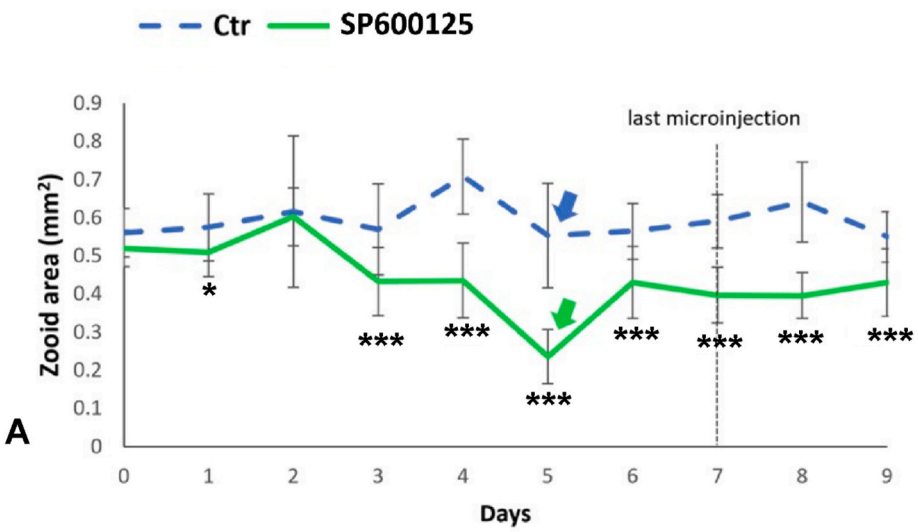

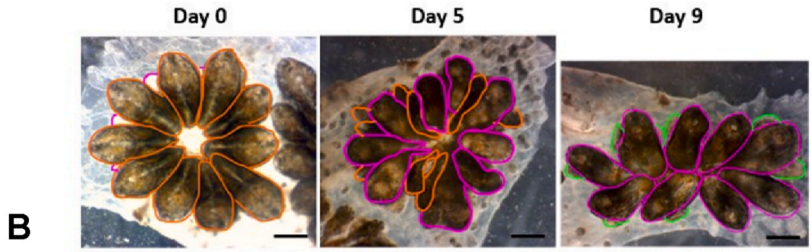

C

C vs treated		
day	*p*-value	degrees of freedom
0	0.129	36
1	**0.012**	36
2	0.767	36
3	**< 0.001**	36
4	**< 0.001**	36
5	**< 0.001**	36
6	**< 0.001**	36
7	**< 0.001**	36
8	**< 0.001**	36
9	**< 0.001**	36

Fig. 8. (A) Mean area of adult zooids in *B. schlosseri* colonies microinjected with SP600125 (solid line) or FSW containing 0.1% DMSO (control, dashed line) over a one-week experimental period. TO (indicated by arrows) occurred on day 5 in both SP600125-treated and control colonies. The final microinjection was administered on day 7. Asterisks indicate statistically significant differences between SP600125-treated and control colonies at the corresponding time points (*: $p < 0.05$; ***: $p < 0.001$). (B) Representative colony treated with SP600125 and monitored throughout the experiment. Different colors identify successive zooid generations: orange (first generation), purple (second generation), and green (third generation). Scale bars = 0.5 mm. (C) Summary table of the statistical comparisons between control and SP600125-treated colonies. (For interpretation of the references to color in this figure legend, the reader is referred to the Web version of this article.)

were downregulated following PD98059 and SP600125 treatments.

To investigate whether oxidative stress can modulate *Botryllus* MAPK transcription, colonies were exposed to Cu^{2+}, Zn^{2+}, and Cd^{2+}, all known inducers of oxidative stress in ascidians [50,67,68], and the expression of *bsmapk-1* and *bsmapk-8* was analysed. All three metals affected MAPK transcription, though with distinct patterns. These differential responses likely reflect the higher toxicity of cadmium compared with Cu^{2+} and Zn^{2+}. As a non-essential metal, Cd^{2+} requires specific detoxification mechanisms, including haemocyte-mediated scavenging, as previously described in *C. robusta* [96]. Although we did not directly assess apoptosis or cell proliferation in this study, the temporal expression pattern suggests possible differential and time-dependent involvement

of *bsmapk-8* and *bsmapk-1*, which warrants further investigation. In mammalian cells, Cd^{2+} induces the activation of both ERK and JNK [97, 98], in agreement with our observations. Similar activations of MAPK pathways have been reported also for copper [99] and zinc [100]. Notably, the early rise in *bsmapk-8* transcription relative to *bsmapk-1* during exposure to Cu^{2+} and Cd^{2+} suggests a differential temporal regulation of these kinases, potentially reflecting distinct roles in stress response dynamics rather than a strictly sequential functional cascade. This may indicate that *bsmapk-8* is preferentially associated with early stress signalling, whereas *bsmapk-1* may be involved in later recovery or homeostatic processes, although functional validation will be required to support this interpretation.

Since phagocytosis is essential for the removal of effete cells during TO and for the normal progression of the colonial blastogenetic cycle [57], and phagocytes are negatively affected by MAPK inhibitors, we next examined the effects of microinjecting the two inhibitors on the blastogenetic cycle. The results show that prolonged treatment with the inhibitors reduced both the size and number of zooids, induced malformations in zooids and buds, and prevented budlet formation. In the case of PD98059, the TO occurred earlier than in control colonies. Our results are consistent with those of Rosner et al. [101], who suggested a role for ERK in bud development.

Taken together, our results indicate that MAPK-driven signalling pathways may play a key role in sustaining the progression of the colonial blastogenetic cycle. In addition, the potential regulatory roles of MAPKs on SG proteins and antioxidant enzymes, require further validation, as these interactions may coordinate stress responses and proliferative processes during the blastogenetic cycle, thereby contributing to colony renewal. Furthermore, our findings suggest that MAPK pathways may act as integrative signalling modules, linking environmental and cellular stress signals to coordinate appropriate physiological responses. These insights lay the groundwork for exploring the evolutionary conservation of MAPK-mediated regulation of immune and stress responses in chordates.

Ethical approval

No approval of research ethics committees was required to accomplish the goals of this study because experimental work was conducted with an unregulated invertebrate species.

Credit author statement

Loriano Ballarin: Conceptualization, Funding acquisition, Resources, Writing-review & Editing, Supervision. Laura Drago: Methodology, Formal analysis, Investigation, Writing-original draft. Writing-review & Editing. Francesca Frisoni: Methodology, Formal analysis, Investigation, Writing-review & Editing. Gianfranco Santovito: Resources, Writing-review & Editing.

Competing interests

The authors have no relevant financial or non-financial interests to disclose.

Acknowledgements

This work was supported by a grant (DOR 2024) from the Department of Biology, University of Padova, awarded to L.B.

Appendix A. Supplementary data

Supplementary data to this article can be found online at https://doi.org/10.1016/j.fsi.2026.111584.

Data availability

Data will be made available on request.

References

[1] M.R. Junttila, S.P. Li, J. Westermarck, Phosphatase-mediated crosstalk between MAPK signaling pathways in the regulation of cell survival, FASEB J. 22 (2008) 954–965, https://doi.org/10.1096/fj.06-7859rev.
[2] Y. Ma, J. Nicolet, Specificity models in MAPK cascade signaling, FEBS Open Bio 13 (2023) 1177–1192, https://doi.org/10.1002/2211-5463.13619.
[3] M. Avkiran, M.S. Marber, Feeling the stress: MAPKKK-MAPKK-MAPK signaling cascades in heart failure, J. Mol. Cell. Cardiol. 48 (2010) 283–285, https://doi.org/10.1016/j.yjmcc.2009.10.019.
[4] B.D. Cuevas, A.N. Abell, G.L. Johnson, Role of mitogen-activated protein kinase kinase kinases in signal integration, Oncogene 26 (2007) 3159–3171, https://doi.org/10.1038/sj.onc.1210409.
[5] D.K. Morrison, MAP kinase pathways, Cold Spring Harbor Perspect. Biol. 4 (2012) a011254, https://doi.org/10.1101/cshperspect.a011254.
[6] Y. Zhang, C. Dong, Regulatory mechanisms of mitogen-activated kinase signaling, Cell. Mol. Life Sci. 64 (2007) 2771–2789, https://doi.org/10.1007/s00018-007-7012-3.
[7] M.M. McKay, D.K. Morrison, Integrating signals from RTKs to ERK/MAPK, Oncogene 26 (2007) 3113–3121, https://doi.org/10.1038/sj.onc.1210394.
[8] Y.D. Shaul, R. Seger, The MEK/ERK cascade: from signaling specificity to diverse functions, Biochim. Biophys. Acta 1773 (2007) 1213–1226, https://doi.org/10.1016/j.bbamcr.2006.10.005.
[9] S. Chimnaronk, J. Sitthiroongruang, K. Srisucharitpanit, M. Srisaisup, A. J. Ketterman, P. Boonserm, The crystal structure of JNK from *Drosophila melanogaster* reveals an evolutionarily conserved topology with that of mammalian JNK proteins, BMC Struct. Biol. 15 (2015) 17, https://doi.org/10.1186/s12900-015-0045-1.
[10] D.N. Dhanasekaran, E.P. Reddy, JNK signaling in apoptosis, Oncogene 27 (2008) 6245–6251, https://doi.org/10.1038/onc.2008.301.
[11] G.L. Johnson, K. Nakamura, The c-jun kinase/stress-activated pathway: regulation, function and role in human disease, Biochim. Biophys. Acta 1773 (2007) 1341–1348, https://doi.org/10.1016/j.bbamcr.2006.12.009.
[12] P.P. Roux, J. Blenis, ERK and p38 MAPK-activated protein kinases: a family of protein kinases with diverse biological functions, Microbiol. Mol. Biol. Rev. 68 (2004) 320–344, https://doi.org/10.1128/MMBR.68.2.320-344.2004.
[13] A. Cuadrado, A.R. Nebreda, Mechanisms and functions of p38 MAPK signaling, Biochem. J. 429 (2010) 403–417, https://doi.org/10.1042/BJ20100323.
[14] A. Cuenda, S. Rousseau, p38 MAP-kinases pathway regulation, function and role in human diseases, Biochim. Biophys. Acta 1773 (2007) 1358–1375, https://doi.org/10.1016/j.bbamcr.2007.03.010.
[15] G. Pages, S. Guérin, D. Grall, F. Bonino, A. Smith, F. Anjuere, P. Auberger, J. Pouysségur, Defective thymocyte maturation in p44 MAP kinase (Erk 1) knockout mice, Science 286 (1999) 1374–1377, https://doi.org/10.1126/science.286.5443.1374.
[16] C. Dong, R.J. Davis, R.A. Flavell, MAP kinases in the immune response, Annu. Rev. Immunol. 20 (2002) 55–72, https://doi.org/10.1146/annurev.immunol.20.091301.131133.
[17] G. Huang, L.Z. Shi, H. Chi, Regulation of JNK and p38 MAPK in the immune system: signal integration, propagation and termination, Cytokine 48 (2009) 161–169, https://doi.org/10.1016/j.cyto.2009.08.002.
[18] Y. Liu, E. Shepherd, L. Nelin, MAPK phosphatases: regulating the immune response, Nat. Rev. Immunol. 7 (2007) 202–212, https://doi.org/10.1038/nri2035.
[19] L. Canesi, M. Betti, C. Ciacci, A. Scarpato, B. Citterio, C. Pruzzo, G. Gallo, Signaling pathways involved in the physiological response of mussel hemocytes to bacterial challenge: the role of stress-activated p38 MAP kinases, Dev. Comp. Immunol. 26 (2002) 325–334, https://doi.org/10.1016/s0145-305x(01)00078-7.
[20] N.V. Iakovleva, A.M. Gorbushin, K.B. Storey, Modulation of mitogen-activated protein kinases (MAPK) activity in response to different immune stimuli in haemocytes of the common periwinkle *Littorina littorea*, Fish Shellfish Immunol. 21 (2006) 315–324, https://doi.org/10.1016/j.fsi.2005.12.008.
[21] Y. Sun, L. Zhang, M. Zhang, Li, Y. Li, X. Hu, S. Wang, Z. Bao, Characterization of three mitogen -activated protein kinases (MAPK) genes reveals involvement of ERK and JNK, not p38 in defense against bacterial infection in Yesso scallop *Patinopecten yessoensis*, Fish Shellfish Immunol. 54 (2016) 507–515, https://doi.org/10.1016/j.fsi.2016.04.139.
[22] L.D. Plows, R.T. Cook, A.J. Davies, A.J. Walker, Activation of extracellular signal regulated kinase is required for phagocytosis by *Limnaea stagnalis* hemocytes, Biochim. Biophys. Acta 1692 (2004) 25–33, https://doi.org/10.1016/j.bbamcr.2004.03.002.
[23] D.L. Huffman, L. Abrami, R. Sasik, J. Corbeil, F.G. van der Goot, R.V. Aroian, Mitogen-activated protein kinase pathways defend against bacterial pore-forming toxins, Proc. Natl. Acad. Sci. USA 101 (2004) 10995–11000, https://doi.org/10.1073/pnas.0404073101.
[24] D.H. Kim, N.T. Liberati, T. Mizuno, H. Inoue, N. Hisamoto, K. Matsumoto, F. M. Ausubel, Integration of *Caenorhabditis elegans* MAPK pathways mediating immunity and stress resistance by MEK-1 MAPK kinase and VHP-1 MAPK phosphatase, Proc. Natl. Acad. Sci. USA 101 (2004) 10990–10994, https://doi.org/10.1073/pnas.0403546101.

[25] J.A.T. Young, A. Dillin, MAPping innate immunity, Proc. Natl. Acad. Sci. USA 101 (2004) 12781–12782, https://doi.org/10.1073/pnas.0404890101.
[26] R. Hatanaka, Y. Sekine, T. Hayakawa, K. Takeda, H. Ichijo, Signaling pathways in invertebrate immune and stress response, ISJ-Invertebr, Surviv. J. 6 (2009) 32–43.
[27] M. Boutros, H. Agaisse, N. Perrimon, Sequential activation of signaling pathways during innate immune responses in *Drosophila*, Dev. Cell 3 (2002) 711–722, https://doi.org/10.1016/s1534-5807(02)00325-8.
[28] I. Wojda, P. Kowalski, T. Jakubowicz, JNK MAP kinase is involved in the humoral immune response of the greater wax moth larvae *Galleria mellonella*, Arch. Insect Biochem. Physiol. 56 (2004) 143–154, https://doi.org/10.1002/arch.20001.
[29] D.K. Fabian, M. Fuentealba, H.M. Dönertaş, L. Partridge, J.M. Thornton, Functional conservation in genes and pathways linking ageing and immunity, Immun. Ageing 18 (2021) 23, https://doi.org/10.1186/s12979-021-00232-1.
[30] Y. Wu, X. Zhao, Y. Xiang, M. Guo, C. Li, Evolution of mitogen-activated protein kinase family and their immune function in *Apostichopus japonicus*, Dev. Comp. Immunol. 139 (2023) 104586, https://doi.org/10.1016/j.dci.2022.104586.
[31] F. Delsuc, G. Tsagkogeorga, N. Lartillot, H. Philippe, Additional molecular support for the new chordate phylogeny, Genesis 46 (2008) 592–604, https://doi.org/10.1002/dvg.20450.
[32] T. Stach, J.M. Turbeville, Phylogeny of Tunicata inferred from molecular and morphological characters, Mol. Phylogenet. Evol. 25 (2002) 408–428, https://doi.org/10.1016/S1055-7903(02)00305-6.
[33] B.J. Swalla, A.B. Smith, Deciphering deuterostome phylogeny: molecular, morphological and palaeontological perspectives, Phil. Trans. Roy. Soc. Lond. 363B (2008) 1557–1568, https://doi.org/10.1098/rstb.2007.2246.
[34] F. Cima, F. Caicci, P. Sordino, The haemocytes of the salp *Thalia democratica* (Tunicata, Thaliacea): an ultrastructural and histochemical study in the oozoid, Acta Zool, Stock 95 (2014) 375–391, https://doi.org/10.1111/azo.12034.
[35] F. Cima, F. Caicci, V. Nittoli, R. Marino, F. Crocetta, P. Sordino, Immunological response to bacterial infection in a pelagic tunicate: inflammation in the salp Thalia democratica, J. Invertebr. Pathol. 159 (2018) 28–40, https://doi.org/10.1016/j.jip.2018.10.012.
[36] N. Franchi, L. Ballarin, Immunity in protochordates: the tunicate perspective, Front. Immunol. 8 (2017) 674, https://doi.org/10.3389/fimmu.2017.00674.
[37] L. Ballarin, Ascidian cytotoxic cells: from zero to hero, ISJ-Invertebr, Surviv. J. 20 (2023) 79–88, https://doi.org/10.25431/1824-307X/isj.v20i1.79-88.
[38] M. Cammarata, G. Candore, V. Arizza, C. Caruso, N. Parrinello, Cytotoxic activity of *Styela plicata* hemocytes against mammalian cell targets: II. Properties of the in vitro reaction against human tumour cell lines, Anim. Biol. 4 (1995) 139–144.
[39] L. Lipari, M. Cammarata, V. Arizza, D. Parrinello, Cytotoxic activity of *Styela plicata* hemocytes against mammalian cell targets: I. Properties of the in vitro reaction against erythrocytes, Anim. Biol. 4 (1995) 131–137.
[40] N. Parrinello, M. Cammarata, V. Arizza, Univacuolar refractile hemocytes from the tunicate *Ciona intestinalis* are cytotoxic for mammalian erythrocytes in vitro, Biol. Bull. 190 (1996) 418–425, https://doi.org/10.2307/1543035.
[41] L. Ballarin, F. Cima, A. Sabbadin, Morula cells and histocompatibility in the colonial ascidian *Botryllus schlosseri*, Zool. Sci. 12 (1995) 757–764, https://doi.org/10.2108/zsj.12.757.
[42] B. Rinkevich, S. Tartakover, H. Gershon, Contribution of morula cells to allogeneic responses in the colonial ascidian *Botryllus schlosseri*, Mar. Biol. 131 (1998) 227–236, https://doi.org/10.1007/s002270050315.
[43] F. Cima, A. Sabbadin, G. Zaniolo, L. Ballarin, Colony specificity and chemotaxis in the compound ascidian *Botryllus schlosseri*, Comp. Biochem. Physiol. 145A (2006) 376–382, https://doi.org/10.1016/j.cbpa.2006.07.017.
[44] L. Ballarin, Immunobiology of compound ascidians, with particular reference to *Botryllus schlosseri*: state of art, ISJ-Invert, Surviv. J. 5 (2008) 54–74.
[45] L. Ballarin, Ascidian cytotoxic cells: state of the art and research perspectives, ISJ-Invert, Surviv. J. 9 (2012) 1–6.
[46] O. Goldstein, E.A. Mandujano-Tinoco, T. Levy, S. Talice, T. Raveh, O. Gershoni-Yahalom, A. Voskoboynik, B. Rosental, *Botryllus schlosseri* as a unique colonial chordate model for the study and modulation of innate immune activity, Mar. Drugs 19 (2021) 454, https://doi.org/10.3390/md19080454.
[47] N. Franchi, F. Schiavon, M. Betti, L. Canesi, L. Ballarin, Insight on signal transduction pathways involved in phagocytosis in the colonial ascidian *Botryllus schlosseri*, J. Invertebr. Pathol. 112 (2013) 260–266, https://doi.org/10.1016/j.jip.2012.12.001.
[48] N. Franchi, L. Ballarin, Influence of cadmium on the morphology and functionality of haemocytes in the compound ascidian *Botryllus schlosseri*, Comp. Biochem. Physiol. 158C (2013) 29–35, https://doi.org/10.1016/j.cbpc.2013.04.003.
[49] N. Franchi, F. Ballin, L. Manni, F. Schiavon, G. Basso, L. Ballarin, Recurrent phagocytosis-induced apoptosis in the cyclical generation change of the compound ascidian *Botryllus schlosseri*, Dev. Comp. Immunol. 62 (2016) 8–16, https://doi.org/10.1016/j.dci.2016.04.011.
[50] N. Franchi, D. Ferro, L. Ballarin, G. Santovito, Transcription of genes involved in glutathione biosynthesis in the solitary tunicate *Ciona intestinalis* exposed to metals, Aquat. Toxicol. 114–115 (2012) 14–22, https://doi.org/10.1016/j.aquatox.2012.02.007.
[51] N. Franchi, F. Ballin, L. Ballarin, Protection from oxidative stress in immunocytes of the colonial ascidian *Botryllus schlosseri*: transcript characterization and expression studies, Biol. Bull. 232 (2017) 45–57, https://doi.org/10.1086/691694.
[52] A. Jiang, Z. Yu, C. Wang, Effect of cadmium on the antioxidant system of the ascidian, *Styela clava*, Mar. Biol. Res. 7 (2011) 388–397, https://doi.org/10.1080/17451000.2010.515685.
[53] N. Parrinello, A. Vizzini, V. Arizza, G. Salerno, D. Parrinello, M. Cammarata, F. T. Giaramita, M. Vazzana, Enhanced expression of a cloned and sequenced *Ciona intestinalis* TNFalpha-like (CiTNF alpha) gene during the LPS-induced inflammatory response, Cell Tissue Res. 334 (2008) 305–317, https://doi.org/10.1007/s00441-008-0695-4.
[54] V. Arizza, A. Bonura, L. La Paglia, A. Urso, A. Pinsino, A. Vizzini, Transcriptional and in silico analyses of MIF cytokine and TLR signaling interplay in the LPS inflammatory response of *Ciona robusta*, Sci. Rep. 10 (2020) 11339, https://doi.org/10.1038/s41598-020-68339-x.
[55] L. Drago, G. Perin, G. Santovito, L. Ballarin, The stress granule component TIAR during the non-embryonic development of the colonial ascidian *Botryllus schlosseri*, Fish Shellfish Immunol. 141 (2023) 108999, https://doi.org/10.1016/j.fsi.2023.108999.
[56] L. Drago, T. Sasada, T. Sunanaga, L. Ballarin, Stress granule related-genes during blastogenetic cycle of two colonial ascidians: *Botryllus schlosseri* compared to *Botryllus primigenus*, Dev. Dyn. 254 (2024) 26–39, https://doi.org/10.1002/dvdy.714.
[57] A. Voskoboynik, B. Rinkevich, A. Weiss, E. Moiseeva, A.Z. Reznick, Macrophage involvement for successful degeneration of apoptotic organs in the colonial urochordate *Botryllus schlosseri*, J. Exp. Biol. 207 (2004) 2409–2416, https://doi.org/10.1242/jeb.01045.
[58] L. Ballarin, F. Schiavon, L. Manni, Natural apoptosis during the blastogenetic cycle of the colonial ascidian *Botryllus schlosseri*: a morphological analysis, Zool. Sci. 27 (2010) 96–102, https://doi.org/10.2108/zsj.27.96.
[59] F. Cima, L. Manni, G. Basso, E. Fortunato, B. Accordi, F. Schiavon, L. Ballarin, Hovering between death and life: natural apoptosis and phagocytes in the blastogenetic cycle of the colonial ascidian *Botryllus schlosseri*, Dev. Comp. Immunol. 34 (2010) 272–285, https://doi.org/10.1016/j.dci.2009.10.005.
[60] L. Manni, G. Zaniolo, F. Cima, P. Burighel, L. Ballarin, *Botryllus schlosseri*: a model ascidian for the study of asexual reproduction, Dev. Dyn. 236 (2007) 335–352, https://doi.org/10.1002/dvdy.21037.
[61] A. Peronato, N. Franchi, L. Ballarin, BsTLR1: a new member of the TLR family of recognition proteins from the colonial ascidian *Botryllus schlosseri*, Fish Shellfish Immunol. 106 (2020) 937–974, https://doi.org/10.1016/j.fsi.2020.09.006.
[62] C.L. Kielkopf, W. Bauer, I.L. Urbatsch, Bradford assay for determining protein concentration, Cold Spring Harb. Protoc. 4 (2020) 102269, https://doi.org/10.1101/pdb.prot102269.
[63] U.K. Laemmli, Cleavage of structural proteins during the Assembly of the Head of Bacteriophage T4, Nature 227 (1970) 680–685, https://doi.org/10.1038/227680a0.
[64] K.J. Livak, T.D. Schmittgen, Analysis of relative gene expression data using real-time quantitative PCR and the $2^{-\Delta\Delta CT}$ method, Methods 25 (2001) 402–408, https://doi.org/10.1006/meth.2001.1262.
[65] L. Ballarin, F. Cima, A. Sabbadin, Phagocytosis in the colonial ascidian *Botryllus schlosseri*, Dev. Comp. Immunol. 18 (1994) 467–481, https://doi.org/10.1016/s0145-305x(06)80002-9.
[66] L. Drago, A. Peronato, N. Franchi, L. Ballarin, R. Bakiu, G. Santovito, Stress granules in *Ciona robusta*: first evidences of TIA-1-related nucleolysin and tristetraprolin gene expression under metal exposure, Comp. Biochem. Physiol. 243C (2021) 108977, https://doi.org/10.1016/j.cbpc.2021.108977.
[67] D. Ferro, N. Franchi, V. Mangano, R. Bakiu, M. Cammarata, N. Parrinello, G. Santovito, L. Ballarin, Characterization and metal-induced gene transcription of two new copper zinc superoxide dismutases in the solitary ascidian *Ciona intestinalis*, Aquat. Toxicol. 140–141 (2013) 369–379, https://doi.org/10.1016/j.aquatox.2013.06.020.
[68] D. Ferro, N. Franchi, R. Bakiu, L. Ballarin, G. Santovito, Molecular characterization and metal induced gene expression of the novel glutathione peroxidase 7 from the chordate invertebrate Ciona robusta, Comp. Biochem. Physiol. 205C (2018) 1–7, https://doi.org/10.1016/j.cbpc.2017.12.002.
[69] M. Böhm, V. Gamulin, H.C. Schröder, W.E. Müller, Evolution of osmosensing signal transduction in Metazoa: stress-activated protein kinases p38 and JNK, Cell Tissue Res. 308 (2002) 431–438, https://doi.org/10.1007/s00441-002-0535-x.
[70] D.T. Dudley, L. Pang, S.J. Decker, A.J. Bridges, A.R. Saltiel, A synthetic inhibitor of the mitogen-activated protein kinase cascade, Proc. Natl. Acad. Sci. USA 92 (1995) 7686–7689, https://doi.org/10.1073/pnas.92.17.7686.
[71] B.L. Bennett, D.T. Sasaki, B.W. Murray, E.C. O'Leary, S.T. Sakata, W. Xu, J. C. Leisten, A. Motiwala, S. Pierce, Y. Satoh, S.S. Bhagwat, A.M. Manning, D. W. Anderson, SP600125, an anthrapyrazolone inhibitor of Jun N-terminal kinase, Proc. Natl. Acad. Sci. USA 98 (2001) 13681–13686, https://doi.org/10.1073/pnas.251194298.
[72] L. Yang, L. Mao, H. Chen, M. Catavsan, J. Kozinn, A. Arora, X. Liu, J.Q. Wang, A signaling mechanism from Gαq-protein-coupled metabotropic glutamate receptors to gene expression: role of the c-Jun N-terminal kinase pathway, J. Neurosci. 26 (2006) 971–980, https://doi.org/10.1523/JNEUROSCI.4423-05.2006.
[73] T.K.P. Doan, K.S. Park, H.K. Kim, D.S. Park, J.H. Kim, T.R. Yoon, Inhibition of JNK and ERK pathways by SP600125- and U0126-enhanced osteogenic differentiation of bone marrow stromal cells, Tissue Eng. Regen. Med. 9 (2012) 283–294, https://doi.org/10.1007/s13770-012-0352-6.
[74] T.S. Cohen, G.G. Gladys, A. Khasgiwala, S. Margulies, MAPk activation modulates permeability of isolated rat alveolar epithelial cell monolayers following cyclic stretch, PLoS One 5 (2010) e10385, https://doi.org/10.1371/journal.pone.0010385.
[75] D. Barilá, R. Mangano, S. Gonfloni, J. Kretzschmar, M. Moro, D. Bohmann, G. Superti-Furga, A nuclear tyrosine phosphorylation circuit: c-Jun as an activator

and substrate of c-Abl and JNK, EMBO J. 19 (2000) 273–281, https://doi.org/10.1093/emboj/19.2.273.
[76] N. Nowshin Oishee, M. Marzan, A.O. Olatunji, K.M. Khalid, A. Hasib Shourav, R. E. Noor, A. Kharitonova, A.J. Astalos, J.W. Leahy, M. Acevedo-Duncan, PKC-ι regulates an oncogenic positive feedback loop between the MAPK/JNK signaling pathway, c-Jun/AP-1 and TNF-α in breast cancer, Int. J. Mol. Sci. 26 (2025) 7288, https://doi.org/10.3390/ijms26157288.
[77] T. Kitanaka, R. Nakano, N. Kitanaka, T. Kimura, K. Okabayashi, T. Narita, H. Sugiya, JNK activation is essential for activation of MEK/ERK signaling in IL-1β-induced COX-2 expression in synovial fibroblasts, Sci. Rep. 7 (2017) 39914, https://doi.org/10.1038/srep39914.
[78] K. Zhang, R. Zhang, Y. Zhang, M. Zhang, H. Su, F. Zhao, D. Wang, G. Cao, Y. Zhang, Regulation of LPS-ind uced inflammatory responses in bovine mammary epithelial cells via TLR4-mediated NF-κB and MAPK signaling pathways by lactoferrin, Life 15 (2025) 69, https://doi.org/10.3390/life15010069.
[79] A. Matsuzawa, H. Ichijo, Redox control of cell fate by MAP kinase: physiological roles of ASK1-MAP kinase pathway in stress signaling, Biochim. Biophys. Acta 1780 (2008) 1325–1336, https://doi.org/10.1016/j.bbagen.2007.12.011.
[80] X. Wang, C. Wang, X. Cui, L. Wang, Z. Liu, B. Xu, H. Li, Molecular mechanism by which Apis cerana cerana MKK6 (AccMKK6)-mediated MAPK cascades regulate the oxidative stress response, Biosci. Rep. 38 (2018), https://doi.org/10.1042/BSR20181301. BSR20181301.
[81] A.J. Whitmarsh, A central role for p38 MAPK in the early transcriptional response to stress, BMC Biol. 8 (2010) 47, https://doi.org/10.1186/1741-7007-8-47.
[82] L. Wang, W. Yang, B. Li, S. Yuan, F. Wang, Response to stress in biological disorders: implications of stress granule assembly and function, Cell Prolif. 54 (2021) e13086, https://doi.org/10.1111/cpr.13086.
[83] R. García, V. Pulido, S. Orellana-Muñoz, C. Nombela, C.R. Vázquez de Aldana, J. M. Rodríguez-Peña, J. Arroyo, Signalling through the yeast MAPK cell wall integrity pathway controls P-body assembly upon cell wall stress, Sci. Rep. 9 (2019) 3186, https://doi.org/10.1038/s41598-019-40112-9.
[84] N. Kedersha, P. Anderson, Stress granules: sites of mRNA triage that regulate mRNA stability and translatability, Biochem. Soc. Trans. 30 (2002) 963–969, https://doi.org/10.1042/bst0300963.
[85] W.L. Chang, W.Y. Tarn, A role for transportin in deposition of TTP to cytoplasmic RNA granules and mRNA decay, Nucleic Acids Res. 37 (2009) 6600–6612, https://doi.org/10.1093/nar/gkp717.
[86] M. Piecyk, S. Wax, A.R. Beck, N. Kedersha, M. Gupta, B. Maritim, S. Chen, C. Gueydan, V. Kruys, M. Streuli, P. Anderson, TIA-1 is a translational silencer that selectively regulates the expression of TNF-alpha, EMBO J. 19 (2000) 4154–4163, https://doi.org/10.1093/emboj/19.15.4154.
[87] T. Zhang, V. Kruys, G. Huez, C. Gueydan, AU-rich element-mediated translational control: complexity and multiple activities of trans-activating factors, Biochem. Soc. Trans. 30 (2002) 952–958, https://doi.org/10.1042/bst0300952.
[88] P. Kovarik, F. Ebner, V. Sedlyarov, Posttranscriptional regulation of cytokine expression, Cytokine 89 (2017) 21–26, https://doi.org/10.1016/j.cyto.2015.11.007.
[89] N. Ronkina, N. Shushakova, C. Tiedje, T. Yakovleva, M.A.X. Tollenaere, A. Scott, T.S. Batth, J.V. Olsen, A. Helmke, S.H. Bekker-Jensen, A.R. Clark, A. Kotlyarov, M. Gaestel, The role of TTP phosphorylation in the regulation of inflammatory cytokine production by MK2/3, J. Immunol. 203 (2019) 2291–2300, https://doi.org/10.4049/jimmunol.1801221.
[90] S. Rezatabar, A. Karimian, V. Rameshknia, H. Parsian, M. Majidinia, T.A. Kopi, A. Bishayee, A. Sadeghinia, M. Yousefi, M. Monirialamdari, B. Yousefi, RAS/MAPK signaling functions in oxidative stress, DNA damage response and cancer progression, J. Cell. Physiol. 234 (2019) 14951–14965, https://doi.org/10.1002/jcp.28334.
[91] H.C. Reinhardt, P. Hasskamp, I. Schmedding, S. Morandell, M.A. van Vugt, X. Wang, R. Linding, S.E. Ong, D. Weaver, S.A. Carr, M.B. Yaffe, DNA damage activates a spatially distinct late cytoplasmic cell-cycle checkpoint network controlled by MK2-mediated RNA stabilization, Mol. Cell. 40 (2010) 34–49, https://doi.org/10.1016/j.molcel.2010.09.018.
[92] R. Sugiura, R. Satoh, S. Ishiwata, N. Umeda, A. Kita, Role of RNA-binding proteins in MAPK signal transduction pathway, J. Signal. Transduct. 2011 (2011) 109746, https://doi.org/10.1155/2011/109746.
[93] M. Brook, C.R. Tchen, T. Santalucia, J. McIlrath, J.S. Arthur, J. Saklatvala, A. R. Clark, Posttranslational regulation of tristetraprolin subcellular localization and protein stability by p38 mitogen-activated protein kinase and extracellular signal-regulated kinase pathways, Mol. Cell Biol. 26 (2006) 2408–2418, https://doi.org/10.1128/MCB.26.6.2408-2418.2006.
[94] W. Takabe, R. Li, L. Ai, F. Yu, J.A. Berliner, T.K. Hsiai, Oxidized low-density lipoprotein-activated c-Jun NH2-terminal kinase regulates manganese superoxide dismutase ubiquitination: implication for mitochondrial redox status and apoptosis, Arterioscler. Thromb. Vasc. Biol. 30 (2010) 436–441, https://doi.org/10.1161/ATVBAHA.109.202135.
[95] Y. Ma, L. Zhang, X. Gao, D. Zhu, GPX3 represses pancreatic cancer cell proliferation, migration and invasion, and improves their chemo-sensitivity by regulating the JNK/c-Jun signaling pathway, Exp. Ther. Med. 27 (2024) 118, https://doi.org/10.3892/etm.2024.12407.
[96] N. Franchi, E. Piccinni, D. Ferro, G. Basso, B. Spolaore, G. Santovito, L. Ballarin, Characterization and transcription studies of a phytochelatin synthase gene from the solitary tunicate *Ciona intestinalis* exposed to cadmium, Aquat. Toxicol. 15 (2014) 47–56, https://doi.org/10.1016/j.aquatox.2014.03.019.
[97] L. Chen, L. Liu, S. Huang, Cadmium activates the mitogen-activated protein kinase (MAPK) pathway via induction of reactive oxygen species and inhibition of protein phosphatases 2A and 5, Free Radic. Biol. Med. 45 (2008) 1035–1044, https://doi.org/10.1016/j.freeradbiomed.2008.07.011.
[98] S. De, S. Kanrar, A. Parithathvi, P. Harshitha, H.S. Dsouza, Mechanistic links between cadmium and MAPK pathways leading to neurodegeneration, Neurotoxicol. Teratol. 114 (2026) 107588, https://doi.org/10.1016/j.ntt.2026.107588.
[99] M.L. Turski, D.C. Brady, H.J. Kim, B.E. Kim, Y. Nose, C.M. Counter, D.R. Winge, D.J. Thiele, A novel role for copper in Ras/mitogen-activated protein kinase signaling, Mol. Cell Biol. 32 (2012) 1284–1295, https://doi.org/10.1128/MCB.05722-11.
[100] A. Hönscheid, S. Dubben, L. Rink, H. Haase, Zinc differentially regulates mitogen-activated protein kinases in human T cells, J. Nutr. Biochem. 23 (2012) 18–26, https://doi.org/10.1016/j.jnutbio.2010.10.007.
[101] A. Rosner, G. Alfassi, E. Moiseeva, G. Paz, C. Rabinowitz, Z. Lapidot, J. Douek, A. Haim, B. Rinkevich, The involvement of three signal transduction pathways in botryllid ascidian astogeny, as revealed by expression patterns of representative genes, Int. J. Dev. Biol. 58 (2014) 677–692, https://doi.org/10.1387/ijdb.140114ar.